BeFo
STIFTELSEN BERGTEKNISK FORSKNING
ROCK ENGINEERING RESEARCH FOUNDATION

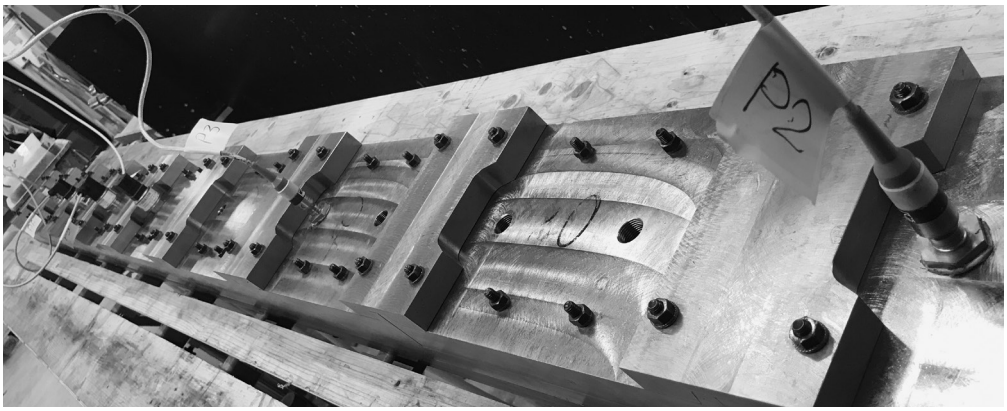

Verification of Real Time Grouting Control (RTGC) theory using an artificial fracture with adjustable aperture order – A numerical and experimental investigation

Giedrius Žirgulis
Liangchao Zou

BeFo Report 252

Cover photo: Test setup and components for RTGC theory experiments. Photo: RISE.

STIFTELSEN BERGTEKNISK FORSKNING
ROCK ENGINEERING RESEARCH FOUNDATION

Verification of Real Time Grouting Control (RTGC) theory using an artificial fracture with adjustable aperture order – A numerical and experimental investigation

Verifiering av RTGC-teori (Real Time Grouting Control) med användning av en artificiell spricka med justerbara spaltvidder – En numerisk och experimentell undersökning

Giedrius Žirgulis

Liangchao Zou

BeFo Report 252
Stockholm 2024
ISSN 1104-1773
ISRN BEFO-R-252-SE

PREFACE

During grouting, insufficient spread of grout within the rock fractures is one of the major issues, which negatively impacts the resulting sealing and service live of underground structures. This study therefore took a novel effort to examine the performance of RTGC theory with aperture variations. The results provided insights of the reliability of the theory.

The reference group consisted of Lisa Hernqvist, Ali Nejad Ghafar, Robert Sturk, Almir Draganović and Patrik Vidstrand.

The study was co-financed by BeFo, SBUF, KTH and RISE.

Stockholm

Patrik Vidstrand

FÖRORD

Vid injektering är otillräcklig spridning av injekteringsbruk i bergsprickorna ett av de stora problemen, vilket negativt påverkar den resulterande tätningen och livslängden för underjordiska strukturer. Denna studie undersökte RTGC-teorin fungerar vid variation i aperturen. Resultaten ger en ökad insikt om teorins tillförlitlighet.

Referensgruppen utgjordes av Lisa Hernqvist, Ali Nejad Ghafar, Robert Sturk, Almir Draganović och Patrik Vidstrand.

Studien samfinansierades av BeFo, SBUF, KTH och RISE.

Stockholm

Patrik Vidstrand

SUMMARY

In cement-based grouting, insufficient spread of grout within the rock fractures is one of the major issues, which negatively impacts the sealing performance and service life of underground structures. On the other hand, an excess of the grout spread is neither economic nor environmentally friendly. Hence, optimization of the grout spread is of the greatest concern in rock grouting to provide the most reliable and economical solution for sealing in the construction and maintenance of underground facilities. Accordingly, the Real Time Grouting Control (RTGC) theory is a method that has been developed to analyse the spread of grout in rock fractures. It predicts the extent of the grout penetration over time based on grout properties and the applied pressure. Despite extensive work conducted to verify the RTGC method in both the lab and the field, it has not yet been sufficiently investigated in the lab under inhomogeneous geometry conditions like a more realistic rock fracture with variable, non-subsequent apertures.

This investigation therefore took a novel effort to examine the performance of RTGC theory at presence of variable aperture constrictions. The idea is to investigate how close are the results of predictions of grout propagation of RTGC theory (at different aperture orders) with the experimental results obtained using an artificial fracture with adjustable aperture order. A fair comparison is further provided between the predicted results and the results of numerical simulations under different aperture distributions. The predictions are obtained using both the hydraulic aperture, the way that the theory was previously used in the early stages of development, as well as the mean-physical aperture, the way that the theory is currently used in the field applications.

An unique equipment, referred to as Variable Aperture Long Slot 2 (VALS II), was designed and produced to meet requirements of this investigation. It consists of multiple short aperture plates attached to a 4m long base plate. The aperture plates have different aperture sizes for representing variable apertures in rock fractures and can be mounted on the base plate in any sequence to form desired aperture size distribution with respect to VALS II inlet for grout inflow.

Test results reveal importance of correct evaluation of grout rheology when applying RTGC theory. Based on them it was concluded that if applying fresh grout rheological properties RTGC theory gave not as precise prediction for grout propagation in time as grout rheological properties at 30 minutes from mixing.

Keywords: Tock grouting; Real Time Grouting Control Theory, Laboratory test; Variable Aperture Long Slot, Variable Aperture Size Distribution, Numerical simulation

SAMMANFATTNING

Vid cementbaserad injektering är otillräcklig spridning av injekteringsbruk i bergsprickorna ett av de stora problemen, vilket negativt påverkar den resulterande tätningen och livslängden för underjordiska strukturer. Å andra sidan är ett överskott av injekteringsbruk varken ekonomiskt eller miljövänligt. Därför är optimering av bruksfördelningen av största vikt vid berginjektering för att tillhandahålla den mest tillförlitliga och ekonomiska lösningen för tätning av underjordiska anläggningar. Real Time Grouting Control-teorin (RTGC) är följaktligen en metod som har utvecklats för att övervaka/förutsäga spridningen av injekteringsbruk i bergsprickor. Den förutsäger omfattningen av injekteringsbrukets inträngning över tiden med hjälp av injekteringsbrukets egenskaper och det applicerade trycket. Trots omfattande arbete som utförts för att verifiera det i både laboratorium och fält, har det ännu inte undersökts tillräckligt i labbet under geometriska förhållanden som en riktig spricka i berg (dvs i en spricka med variabla, icke efterföljande spaltvidder).

Detta projekt tog därför ett nytt försök att undersöka prestandan av RTGC-teorin vid närvaro av förträngningar. Tanken är att undersöka hur nära resultaten av förutsägelser av injekteringsbruksutbredning av RTGC-teorin (vid olika spaltvidder) är de experimentella resultaten som erhålls med användning av en artificiell spricka med justerbara inställningar. En rättvis jämförelse tillhandahålls vidare mellan de förutsagda resultaten och resultaten av numeriska simuleringar under olika spaltvidds fördelningar. Förutsägelserna erhölls med både den hydrauliska spaltvidder, det sätt som teorin tidigare användes i de tidiga utvecklingsstadierna, såväl som den genomsnittliga fysiska öppningen, det sätt som teorin för närvarande används i fälttillämpningar.

Unik utrustning Variable Aperture Long Slot 2 (VALS 2) designades och tillverkades för att uppfylla kraven i denna undersökning. Den består av flera korta spaltviddsplattor fästa på 4m lång basplatta. Spaltviddsplattorna har olika öppningsstorlekar för simulering av bergsprickor och kan monteras på basplattan i valfri sekvens för att bilda önskad spaltviddsstorleksfördelning med avseende på VALS 2-inloppet för injekteringsbruk.

Provningsresultat visade vikten av korrekt utvärdering av injekteringsbruksreologi vid tillämpning av RTGC-teori. Baserat på det drogs slutsatsen att om man applicerade färskt injekteringsbruks reologiska egenskaper gav RTGC-teorin inte lika exakta förutsägelser för injekteringsbrukets utbredning i tid som injekteringsbrukets reologiska egenskaper 30 minuter efter blandning.

Nyckelord: Real Time Grouting Control Teori, Variabel spaltviddsfördelning, Numerisk simulering

CONTENTS

1. INTRODUCTION

One of the major issues in cement grouting is insufficient spread of grout within rock fractures surrounding the underground facility. This deteriorates the sealing and durability performance significantly. On the other hand, unnecessary spread of grout beyond the required penetration length in rock fractures is not sustainable. Therefore, control and optimization of the grout spread in fractures is of the greatest concern in rock grouting to provide a reliable and simultaneously an economical tight-zone around any underground infrastructure.

Over the years, several stop criteria have been proposed to effectively control the grout spread in grouting operations. Among the methods, the real time grouting control (RTGC) theory has been developed by (Gustafson and Stille 1996), (Gustafson and Stille 2005) and further elaborated by (Kobayashi, Stille and Gustafson 2008), (Axelsson, Gustafson and Fransson 2009), (Tsuji, et al. 2012), (Stille, Gustafson and Hassler 2012), (Gustafson, Claesson and Fransson 2013), and (Stille, 2015). The theory predicts the extent of the grout spread over time in rock fractures using the grout rheological properties and the online readings of the pressure during the grouting operations. The theory has been developed based on three fundamental assumptions, from which the uniform fracture aperture is of great importance. Even though there have been some numerical and analytical efforts to study the influence of the fracture geometry on the grout spread (Saeidi, Stille and Torabi 2013), all the associated laboratory investigations have been conducted in either pipes (Håkansson 1993) or parallel plates with uniform aperture (Gustafson, Claesson and Fransson 2013). This means that the theory has not yet been sufficiently investigated in the lab at presence of constrictions and varying apertures similar to the real geometry of a fracture in rock.

Since the physical fracture geometries in rock grouting are unknown and cannot be determined directly, a couple of water tests are normally performed to obtain a rough estimation of the surrounding fracture geometries in the form of hydraulic aperture, b_h. This is the aperture size that was used previously in predictions in the early stages of the development of the RTGC theory. However, according to (Zimmerman and Bodvarsson 1996), (Tsuji, et al. 2012), and (Stille, 2015), it is not the hydraulic aperture that governs the grout take during the grouting operation; it is the fracture's mean physical aperture, b_{phy}. Several investigations have therefore been carried out to find the relationship between b_{phy} and b_h. According to (Stille, 2015), in many cases b_{phy}, which is normally used today in predictions using the RTGC theory, is roughly 2.0 times wider than b_h.

As part of an investigation reported in Ghafar et al. 2024, the authors tried to investigate the influence of variation in apertures in predictions provided by RTGC theory. The project was an experimental investigation conducted using a four-meter-long steel-made artificial fracture, the so-called Varying Aperture Long Slot (VALS). The aim was to verify the RTGC theory for grout flow between two parallel plates with sections with descending apertures of 230-10 μm, which anticipated being more similar to a real

fracture in rock compared to the parallel plates with uniform aperture. The study was mainly based on a comparison between the analytical and the experimental results. The predictions were carried out using the estimated b_{phy} and b_h of VALS between the inlet and outlet. Unfortunately, since there was no possibility to change the distribution and order of the apertures in VALS, the study was not conclusive as anticipated. That was because VALS had been designed and built for other objectives than verification of RTGC theory.

As literature review shows the investigation of RTGC theory in laboratory conditions were done using plates with uniform apertures, pipes or artificial aperture apparatus with fixed aperture distribution. However, these laboratory investigations could not provide insight on RTGC theory predictions in presence of more complex constrictions during grout flow. Moreover, it is not clear if the predictions are governed by b_{phy} or b_h of the artificial fracture in the laboratory test. Therefore, this project aims to investigate RTGC theory for multiple versions of aperture distributions in a laboratory conditions.

As the method for the RTGC theory performance investigation will be used a novel apparatus representing artificial fracture with a variable aperture and with adjustable distribution of apertures. During experiments b_{phy} and b_h of the apparatus will be determined and a grout propagation will be measured. Then experimentally measured grout propagation will be compared to RTGC theory predictions for b_{phy} and b_h. A numerical simulation of the apparatus with then provide the opportunity of verifying the analytical and experimental evaluations in various geometrical conditions.

The objective of this project is to verify the reliability of RTGC theory (both experimentally and numerically) to predict the grout propagation in the artificial fracture with variable aperture.

The scope of the project is:

1. To design and build a new version of VALS with adjustable aperture distribution.
2. To experimentally evaluate the reliability of RTGC theory in prediction of the grout propagation at presence of constrictions. The idea is to investigate how close are the results of predictions of grout propagation of RTGC theory (at different aperture orders) with the experimental results.
3. To verify the performance of the theory at different distribution of apertures using a numerical simulation of the grout flow through the apparatus. A comparison is provided between the predicted results and the results of numerical simulations under different aperture constellations.
4. To investigate how well b_h or b_{phy} is employed in the RTGC theory to predict the grout propagation in the artificial fracture with various aperture distribution. This is to examine which option provides more realistic results.

2. MATERIAL AND METODS

2.1 Design of Variable Aperture Long Slot II (VALS II)

The design of a new version of Variable Aperture Long Slot II (VALS II) was based on experience using the older version of VALS for laboratory research (Ghafar, et al. 2017). The VALS provided possibility to examine grout flow through artificial apertures distributed over 4 meters distance, creating conditions similar to fractures in the rock mass. However, its main limitation was fixed aperture size distribution, that is the aperture size was gradually decreasing from large to small. With the new design of VALS II this limitation was eliminated by introducing concept of short modular aperture plates placed on a 4-meter-long base plate. In this way, the aperture size distributions can be adjusted according to research needs. Moreover, extra aperture plates can be manufactured separately, to replace damaged plate or to introduce new aperture size. Therefore, more versions of aperture distribution can be tested using VALS II compared to the previous version of VALS.

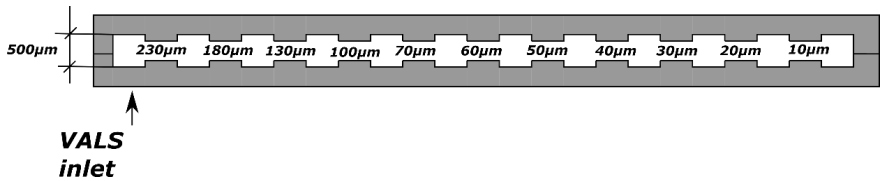

Figure 1. Schematic picture of older version of VALS with fixed aperture distribution.

The other disadvantage of VALS test setup is difficulty in its operation due to heavy weight of top plate. Which means, that for servicing the rig (prepare for testing, cleaning after testing) a lifting machinery needs to be used. Since in VALS II design modular plates represents just one aperture size they become short and therefore light enough for handling by hands.

During design process of VALS II, the simplicity of manufacturing and cost efficiency was also considered. For that reason, two versions of VALS II design were considered Design version 1 and Design version 2

2.1.1 Design version 1

This version aimed for reducing of production costs and time by utilising 4-meter-long plate from older version of VALS. It would serve as a baseplate; only top aperture plates would be manufactured newly (Figure 2). Layout of top aperture plates was adjusted according to existing geometry of the bottom plate, therefore this version had possibility to fit less aperture plates (10 plates) compared to 11 plates of the Design version 2.

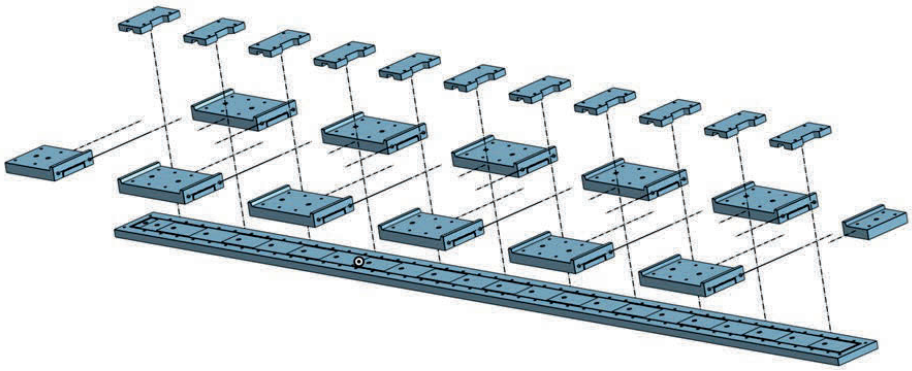

Figure 2. Design version 1 with bottom plate from older VALS.

2.1.2 Design version 2

The Design version 2 consisted of all new components (Figure 3). This design featured slightly longer bottom plate therefore 11 aperture plates could be mounted on it.

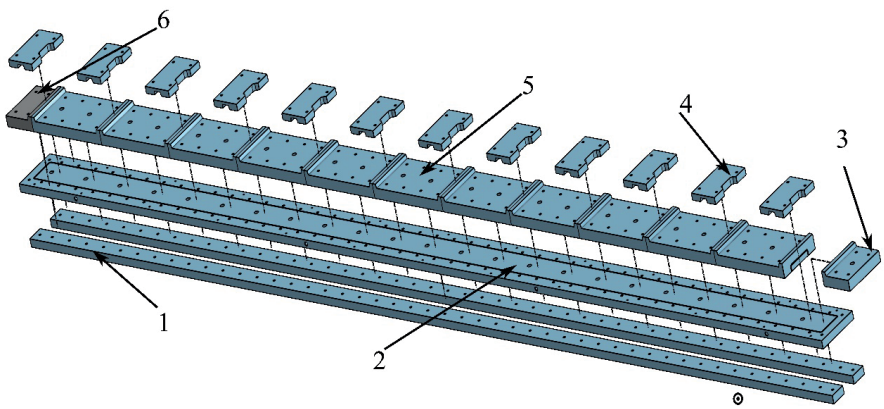

Figure 3. Desing version 2 with all new components: 1- stiffness ribs, 2- bottom plate, 3- inlet plate, 4- tie plates, 5- aperture plates, 6 outlet plate.

2.1.3 Final version for production and specifications

After receiving quotations from producers and a discussion with working group members it was decided that most optimal solution was production of all new components.

The final length of VALS II was 4230mm and width of 210mm. It consisted of following components:

- Two stiffness ribs in the bottom (item 1 in Figure 3). Their purpose to increase stiffness of the VALS II during experiments with grout under pressure.
- Bottom plate (item 2 in Figure 3). It serves as the base on which top aperture plates are mounted. The bottom plate has flat surface machined with pression of ±10µm, a groove for placing O ring seal and multiple holes for attaching valves under VALS II for grout outflow. Location of the valves can be freely selected and holes what are not in use can be plugged with ½-inch blinding plugs.
- Inlet and outlet plates (items 3 and 6 in Figure 3) are for sealing both ends of VALS II rig. Th inlet plate also has a hole for pressure sensor and a hose coupling for grout inflow.
- Aperture plates (item 5 in Figure 3). These are the plates what have machined gap with certain depth, which is called aperture size. The aperture size is machined with precision of 10µm. Features of aperture plate is shown in Figure 4 and consist of:
    - flat surface (1) perpendicular to bottom plate and is the surface which presses to O-ring seal of adjacent plate to make sealed connection between aperture plates.
    - Bolt holes (2) are for tightening aperture plates to bottom plate and stiffness ribs.
    - Threated openings (3) are for placing pressure sensor, if not in use they are sealed with blinding plug.
    - Flanges (4) of aperture plate are for tightening adjacent plates together using tie plates.
    - Pockets with depth of 500µm (5) are for simulating uneven surface of rock fractures.
    - Aperture area (6) where the aperture with desired size is formed when aperture plate is tightly bolted to bottom plate.
    - Precision machined (±10µm) flat surface (7) is the contact area between aperture plate and bottom plate, these two surfaces must be in good contact to ensure correct aperture size during test.
    - The groove (8) is for placing O-ring to seal two adjacent plates.
    - Location pin hole (9) is for correct placing of aperture plate on bottom plate.
- Tie plate (item 4 in Figure 3) are for tightening two aperture plates in longitudinal direction by contact with flanges of aperture plates (Figure 4 (a) 4).

The grout tightness between all components in VALS II is achieved with 5mm diameter O-rings: one long O-ring installed in bottom plate before assembly and multiple short O-rings placed in between aperture plates during assembly of VALS II. The O-rings have shore hardness of 60.

The detailed drawings with dimension of all components are provided in the Appendix section.

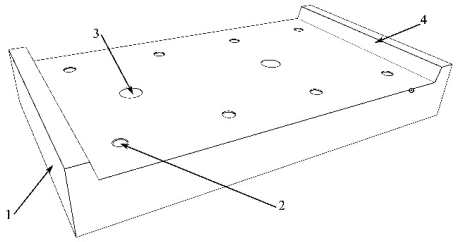

a

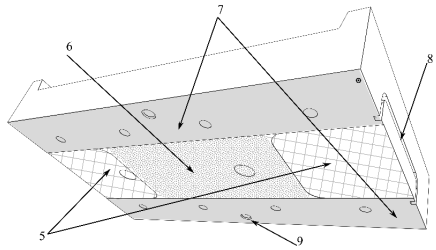

b

Figure 4. Aperture plate: top view (a) and bottom view (b). Here:1- is a side flat surface, 2- holes for tightening bolts, 3- holes for pressure sensor, 4- flanges for tightening adjacent plates together with tie plates, 5- pockets of 500µm size, 6- aperture area, 7- flat surface area, 8- groove for O-ring seal, 9- holes for locating pins.

To operate aperture plates during assembly of VALS II and cleaning it after experiment a lifting magnet was used (Figure 5).

Figure 5. Lifting magnet for handling aperture plates.

2.2 Test setup and first trials

After production of VALS II the setup for experiments on RTGC theory was established and trial test were run with water and grout to check the water and grout tightness and functionality of VALS II.

2.2.1 RTGC test setup

The sketch of test setup is presented in Figure 6a and the picture of assembled VALS II in Figure 6b. The setup consisted of following components:

- Nitrogen bottle which served as source of 200 bar pressure.
- Pressure regulator which was used for reduction of pressure in grout to 11 bar.
- Distribution unit. It is a steel tank designed to withstand high pressure. It has capacity of 12 litres and was filled with grout which then was pressurised using nitrogen.
- VALS II rig assembly with certain aperture distribution. The assembly is done by tightening outlet plate first (Figure 3 item 6), followed by gradual tightening of aperture plates (item 5 in Figure 3) and tie plates (item 4 in Figure 3).
- Pressure sensors installed in top aperture plates. They were used to record grout front propagation speed.
- Mass sensor was located under VALS II outflow valves (Figure 6c). Mass sensor was fixed to movable stand, and a steel bucket was attached to the mass senor. During experiment, mass sensor was used to quantify grout flow rate through each aperture.
- Data Acquisition System (DAQ) us used to record signals from all sensors.

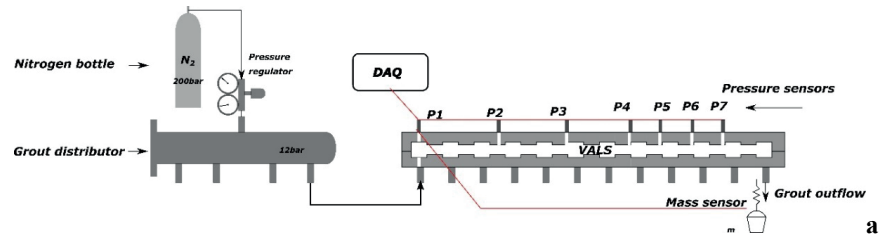

b

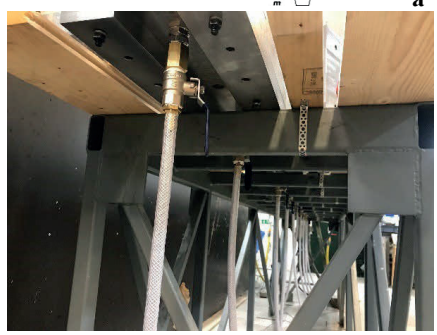

c

Figure 6. Test setup and components for RTGC theory experiments (a), view of assembled VALS II with pressure sensor installed (b) and grout outlet valves installed under VALS II (c).

2.2.2 First trials and setup improvements

First test with water revealed multiple leakage through O-ring seals between aperture plates, aperture plates and bottom plates, also blind plugs and valve threads (Figure 7).

Figure 7. Example of detected leakage in aperture plate.

The leakage problem was solved by changing hardness value of O-ring seals and reinstalling problematic valves and blinding plugs. By experimental approach it was determined that O-rings with Shore hardness of 60 worked best. Diameter of cross-section of O-rings was chosen to be 5mm.

It was also detected that when using locating pins for mounting aperture plates friction force appeared between locating pins and hole in the aperture plate. This friction appeared due to expansion force of compressed O-ring seal between two plates (Figure 8). Due to this effect, it was difficult to remove aperture plates after experiment. Therefore, only two location pins (located under outlet plate see item 6 in Figure 3) were used during subsequent assemblies. It was noticed that by gradual tightening of bolts it was possible to maintain coaxial orientation of aperture plates with respect to bottom plate even without presence of locating pins.

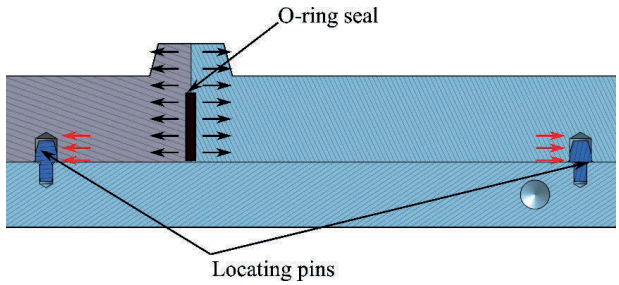

Figure 8. The friction in locating pins created by expansion force of O-ring seal.

When grouting rock fractures cement grain build up can occur at fracture constriction, which leads to forming a stable arch over the constriction. This process is called plug-buildup or filtration (Draganović and Stille 2011).

This problem was observed when grouting tests on VALS II started. Filtration was related to location of grout inlet coupling (Figure 9a) which created air pocket opposite to the grout flow direction. Assumingly the air pocket could have act as trigger for filtration process, which started to occur almost in - all grouting experiments as an immediate grout filtration in the inlet plate after grout inlet valve from distribution unit was opened (a Flash filtration). This led to immediate grout flow stop due to clogged VALS II inlet (Figure 9b). Therefore, the inlet position was changed as shown in Figure 9c. This improved the flash filtration problem. Moreover, the pressure sensor at the inlet remained at its initial position therefore it was still possible to record the pressure of grout exactly at the VALS II inlet.

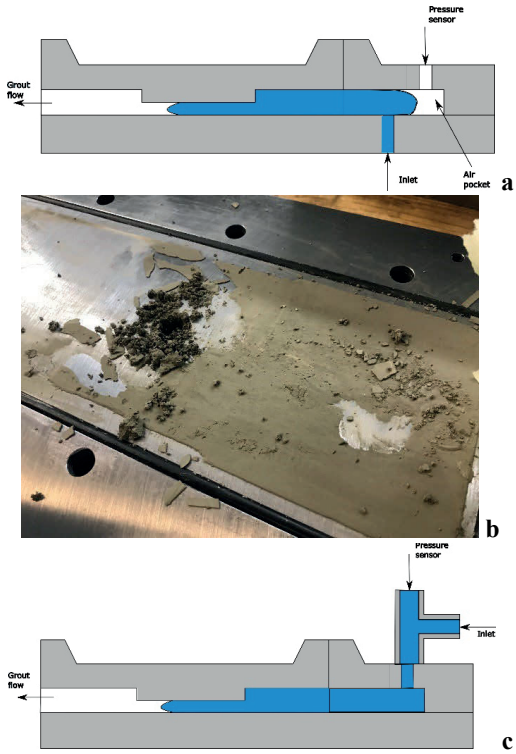

Figure 9. Optimization of position of grout inlet: a- grout inlet from bottom of VALS and location of air pocket under pressure sensor, b- example of grout filtration under pressure sensor and the clogged inlet hole, c- repositioned grout inlet using T-shape coupling.

2.3 Experiments for testing RTGC theory

2.3.1 Aperture distribution alternatives

Five aperture distribution alternatives were considered (Figure 10).They were designed to reflect the various versions of the top plates distribution to simulate uneven fracture distribution.

The alternative A1 starts from a large aperture (120µm) then aperture sizes gradually decrease with sudden increase in the aperture size with a peak value of 140µm near the outflow plate and a fall back to small apertures.

The alternative A2 has gradually decreasing aperture distribution similarly as in VALS.

The alternative A3 has gradually increasing size distribution with a peak towards end of the VALS II followed by a sudden fall of aperture sizes.

The alternative A4 distribution begins similarly as in A3 but with an aperture size peak placed at the middle of VALS II.

The alternative A5 represents a random aperture size distribution. It should be noted that the apertures of 60 µm, 50µm and 40µm were deliberately moved towards end of VALS II to reduce filtration risk at grout inlet plate.

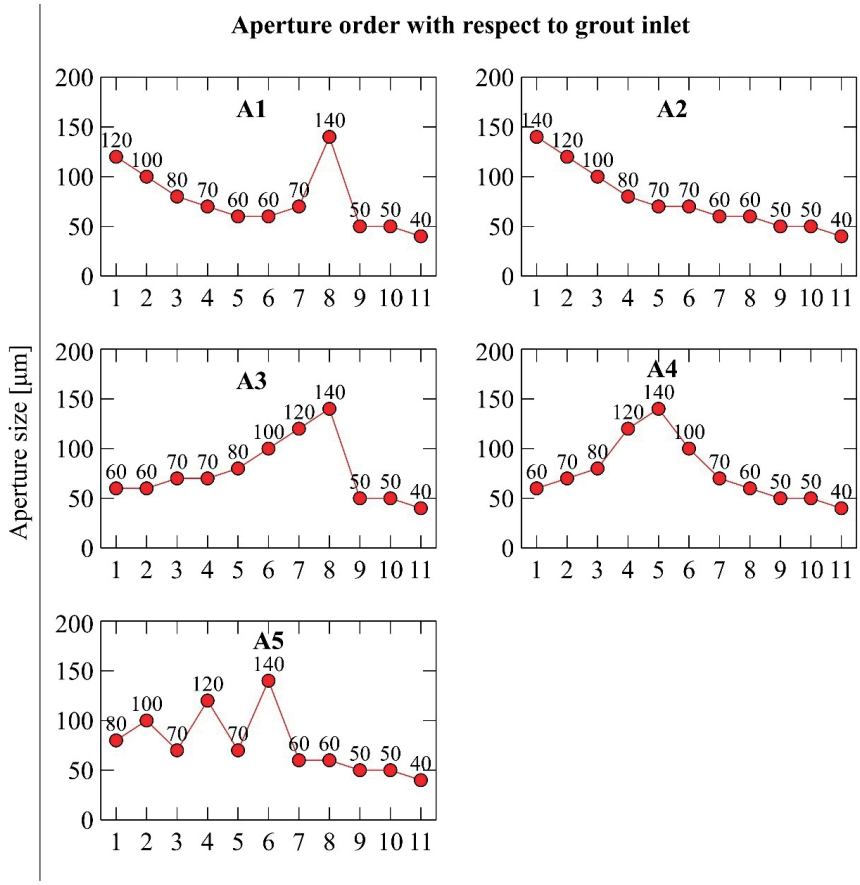

Figure 10. Aperture distribution alternatives.

After discussions with the working group, the following aperture distribution versions were prioritized: A2, A5, A1. Alternative A2 was prioritized due to its similarity to VALS tests conducted in the previous research (Ghafar 2017).

All alternatives were tested with water test and grout test. Both water and grout test were performed three times on each alternative for checking repeatability. A successful water test was considered when no major leakage at VALS II was observed, while a successful grout test was considered when no grout filtration occurred. As shown in results, the filtration phenomenon is a considerable problem (see section 5.1) since the experiment must be stopped once the filtration occurs.

2.4 Materials and mixing

Binder used for the grout was cement MP650 and the plasticizer was Glenium 151. The grout recipe is shown in Table 1. Materials (binder and water) were stored in 5°C climate room and were delivered to mixing station right before the test. The experiment program started with Recipe 1 which in second half of experiments was slightly adjusted to Recipe 2. It should be noted that single recipe was intended to be used in the experiments. However, due to frequent filtration when testing the alternative A2 (see section 3.1) the mix was modified to w/c=1.1 to reduce the risk for filtration.

Table 1. Recipe of grout mix.

	Recipe 1	Recipe 2
w/c	1.0	1.1
Cement	MP650	MP650
Superplasticizer Glenium 151	1.0%	0.8

The grout was mixed using high shear rate laboratory mixer. Typical batch size consisted of 3 kg of cement and water according to recipe. Mixing routine was following:

1. Adding water and plasticizer into mixer.
2. Setting mixing speed to 2000rpm. and adding cement during within 1 minute.
3. Setting mixing speed to 5000rpm and mixing the grout for 4 minutes.

The grout properties (marsh cone time, filter pump, and mud balance) were tested after receiving a new cement batch; however, the grout rheology was monitored during each experiment. The rheology was measured with a laboratory viscometer Brookfield DV2T.

Table 2. Properties of fresh mixed grout.

	0 minutes	10 minutes	30 minutes
Marsh cone time	32.2 sec	32.5 sec	35.7 sec
Filter pump:			
40	50ml	-	-
63	300ml	-	-
Mud balance	1.475g/cm3	-	-

2.5 Experiment routine

The experiment routine consists of following steps:

1. Assembly of VALS II.

2. Connecting grout inlet hose, nitrogen bottle, pressure and mass sensors, distribution unit preparation.
3. Grout mix preparation in high shear rate mixer.
4. Filling grout into distribution unit and pressurising the grout to 10bar. Sample of grout mix is left for measuring grout viscosity, marsh cone time and mud balance test. Grout viscosity was measured at 0, 10, 20 and 30 minutes after mixing.
5. Opening the grout inlet valve in VALS II. Usually at this moment a grout was 5-7 minutes age after mixing.
6. Recording the data from sensors.
7. Stopping the test, depressurising distribution unit.
8. Disassembly of VALS II and distribution unit and cleaning.

It should be noted, when grout starts to flow into VALS II, pressure sensors detect pressure increase based on which grout front propagation is determined. At this point all aperture valves below VALS II are closed (Figure 6b) except the last valve below outlet plate (Figure 3 item 6). The mass sensor with bucket is located under this valve, and when grout reaches end of VALLS II mass sensor starts to record grout flow rate. However, if due to grout penetrability grout doesn't reach outflow valve the mass sensor with bucket is moved to next aperture plate valve towards VALS II inlet. This step is repeated until aperture with constant grout flow is found.

Water test for determining hydraulic aperture b_h of each aperture distribution alternatives was performed in similar manner as the routine described above: distribution unit was filled with water and pressurised to 10bar. The flow rate was measured at the outlet of VALS II with mass sensor and this data then was used for calculation of b_h. The water flow rate was recorded at other apertures as well, by moving mass sensor towards inlet and opening an outflow valve under each aperture.

The results of water and grouting tests were used as follows:

- a water flow rate at VALS II outlet and a grout propagation over time results were used for evaluation of RTGC theory.
- a water and a grout flow rate at each aperture was used as a basis to judge on VALS II assembly and test repeatability (if the sizes of apertures are constant for each test).

3. LABORATORY TEST RESULTS

The test results of aperture distribution alternatives A2, A5 and A1 here are presented in chronological order.

3.1 Filtration problem

As it was described in chapter 3.2 during grouting test filtration occurred quite often. Although the grout inlet position was improved (Figure 9c), this problem was still present at each alternative test (Table 3).

Table 3. Number of tests performed for each aperture distribution alternative for achieving three successful test results.

Alrernative	Test number of experiments to achieve successful 3 tests	Success rate
A2	10	30%
A5	5	60%
A1	5	80% *

* Here only 1 test had filtration and 1 test had grout leakage due to assembly issues, therefore it was not counted in to success rate.

Most often, filtration occurred at the inlet of VALS II in the area where 500µm size pocket (Figure 4, item 5) bordered with smaller sized aperture of an aperture plate (Figure 11).

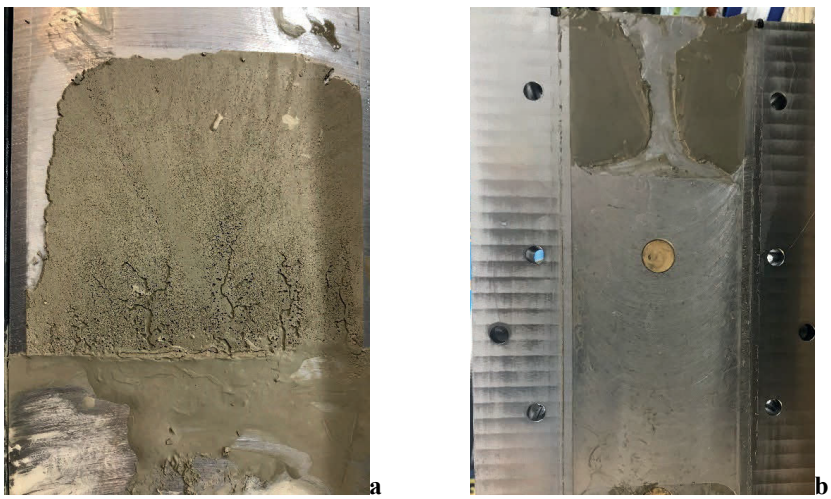

a **b**

Figure 11. Typical grout filtration during experiment: full filtration (a) and partial filtration (b)

The filtration was observed in other aperture plates further away from inlet as well, however it was not that often and consisted of partial filtration (Figure 11 b) mostly.

On one hand side the filtration occurred in expected area, that is where constriction is formed by change of aperture size from 500µ to e.g. 80µm as at the inlet of A5 (Figure 4 A5). On the other hand, the aperture distribution A5 has several small size apertures (80µm and 70µm) located near the inlet of VALS II, which creates large constriction at transition from 500µm pocket and therethore should act as trigger for filtration. Due to this A5 would be expected to have more filtration occurances compared to A1 and A2. However as results show the most often filtration occured at A2 (Table 3), where apertures are distributed from largest to smallest.

During experiments the effect of grout release speed from pressurised distribution unit to VALS inlet was tested. The filtration was randomly occurring in both cases, i.e. when grout valve was opened gradually or at fast rate. Moreover, in some tests the hose connecting distribution unit and VALS II inlet was prefilled with grout prior to test. This did not prevent random filtration occurrence either.

The cement batch was same for all alternatives testing, however recipe 1 (Table 1) with w/c=1.0 was used to test A2 and recipe 2 (w/c=1.1) was used to test A5 and A1.

When comparing test results of A5 and A1 where grout with same w/c ratio was used, A5 has less successful test ratio compared to A1 probably due to larger constrictions at the grout inlet. For the alternative A2 however, the aperture distribution begins with the largest aperture (140µm), i.e. this alternative has smallest constrictions near the inlet and therefore would be expected to have least filtration. However, the results showed largest filtration amount compered to A1 and A5, therefore, it can be assumed that lower w/c might be possible explanation for higher filtration rate for experiments on the aperture distribution alternative A2. However more tests should be performed to confirm the assumptions above and filtration analysis was not in the scope of this research.

3.2 Measured water and ground flow rate

3.2.1 Aperture distribution A2

Seven water tests were performed to gather data of three successful tests. The results are shown in Figure 12. As results show the water flow rates are similar at all three successful test repetitions, especially flow rate is almost equal at small apertures (Figure 12b), since the flow rate at last aperture was used for b_h.calculations.

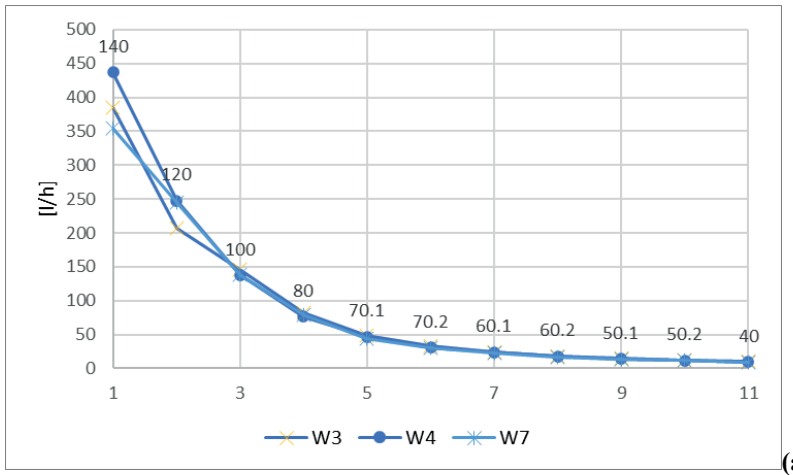

(a)

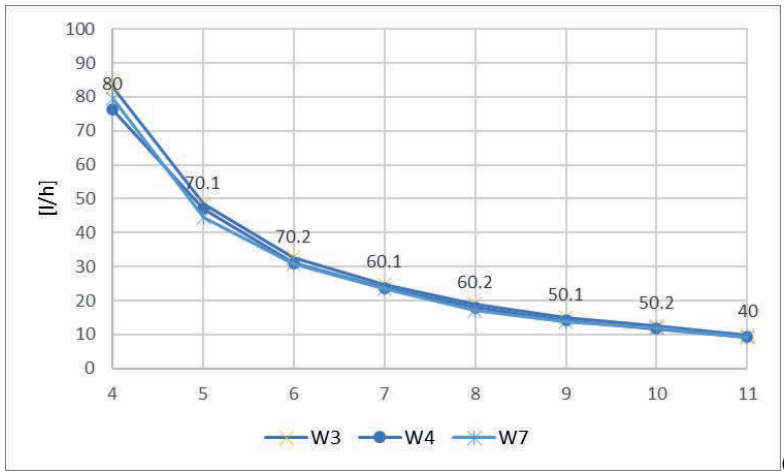

(b)

Figure 12. The water flow rate at each aperture of A2: the graph for all apertures (a) and graph for small apertures at the end of VALS II (b).

For grouting tests however only G5 and G9 had unhindered flow in all apertures. The other tests had filtration in certain apertures (see flow rate of G10 at aperture 5 and G6 at apertures 8 and 9 in Figure 13b). Nevertheless, similar flow rate of the successful flow test sections (see flow rates of G10 at apertures 1, 2, 3, 4, 6, 7, 8, 9, 10, 11 and G6 at apertures 1,2,3, 4, 5, 6, 7, 10, 11 in Figure 13a and b) in graphs show good repeatability of the tests.

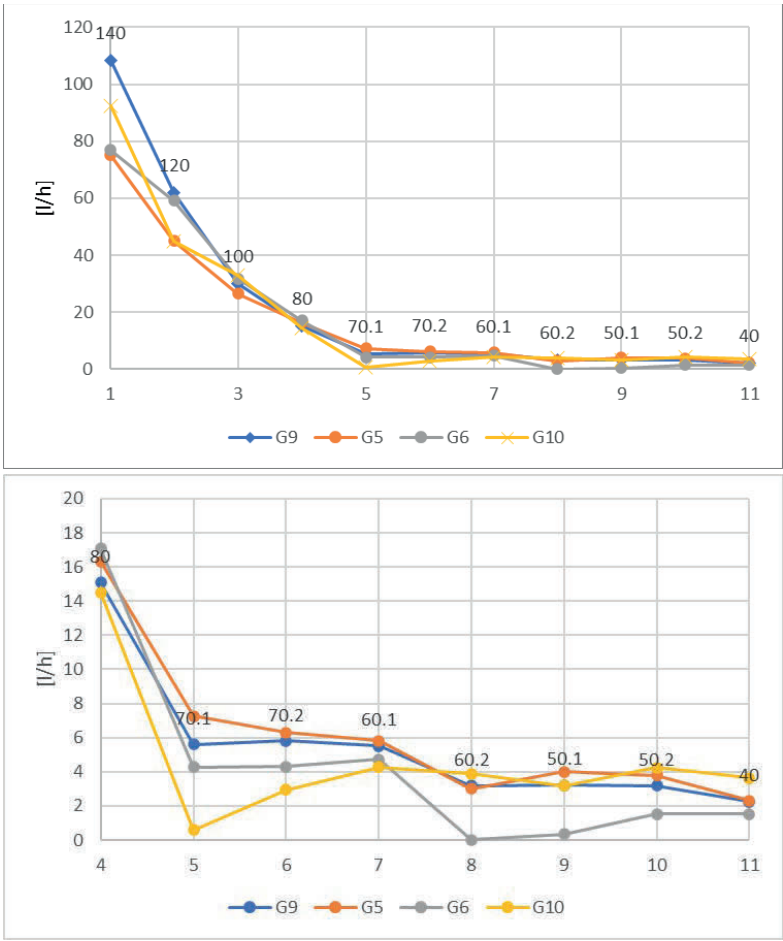

Figure 13. The grout flow rate of successful tests at each aperture of A2: the graph for all apertures (a) and graph for small apertures at the end of VALS II (b).

In experimental data of grout front propagation over time G10 showed slower grout propagation (Figure 14a). This can be explained by grout leakage which occurred at

junction of the aperture plates 4 and 5, i.e. at distance of 1600mm from the inlet. As it can be seen from graph (see Figure 14a), until this point grout propagation during G10 test follows trend of the other tests and after passing a pressure sensor at distance of 1676mm the grout propagation graph starts to deviate from it. Therefore, G10 propagation result was excluded from average value calculations (Figure 14b).

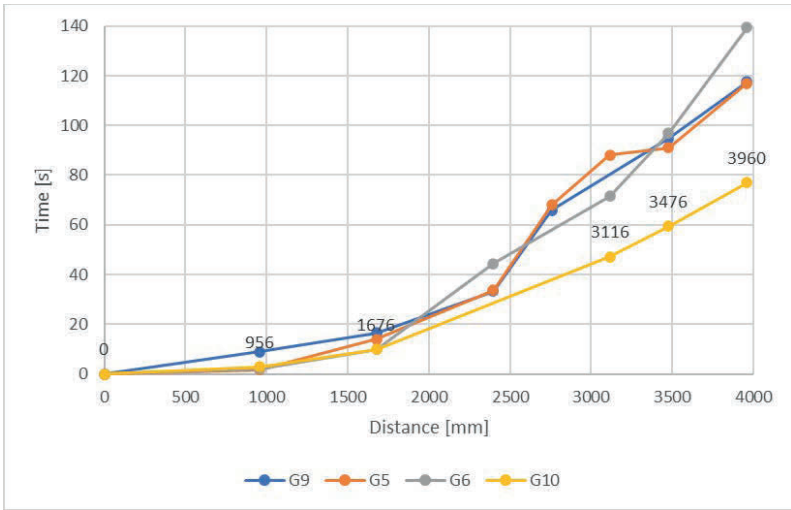

(a)

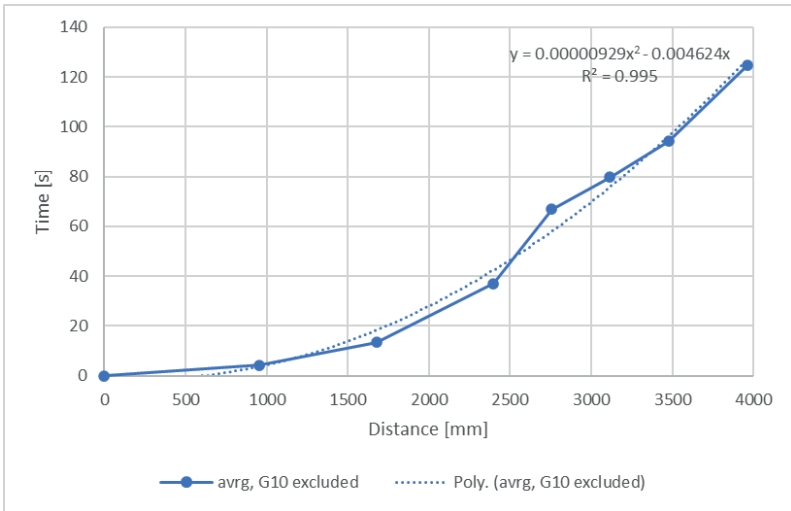

(b)

Figure 14. Recorded grout front propagation A2: the graph for all tests (a) and average values with fitted function with excluded recorded time values for G10 test (b).

3.2.2 Aperture distribution A5

For A5 water test average flow rate calculation W3 result was excluded, the other test performed with good repeatability in both, large and small apertures (Figure 15).

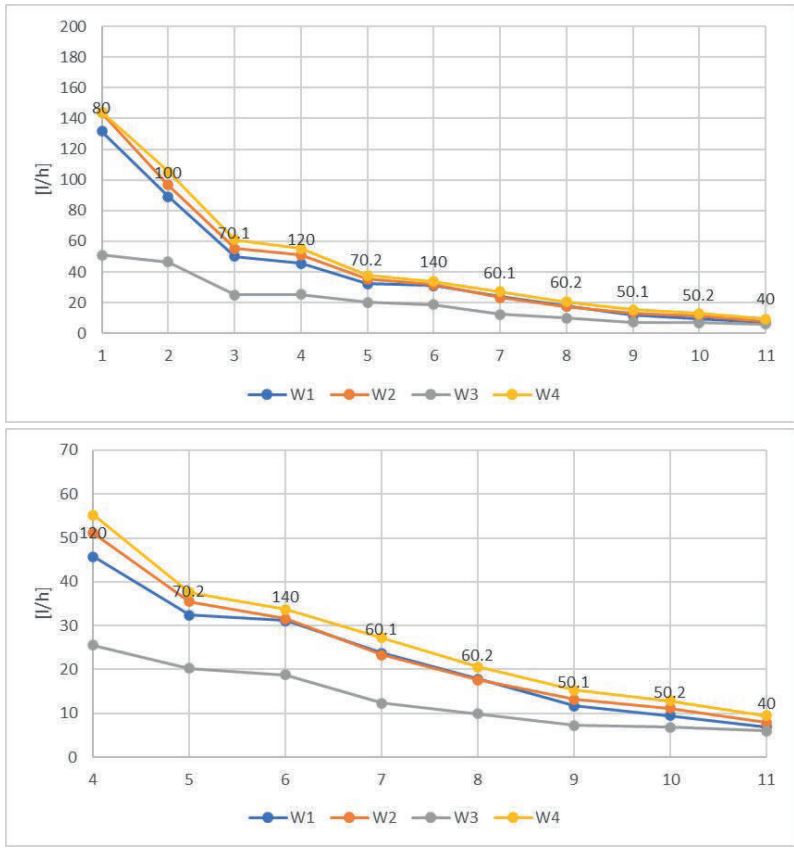

Figure 15. The water flow rate at each aperture of A5: the graph for all apertures (a) and graph for small apertures at the end of VALS II (b).

When measuring grout flow rate at each aperture for test repeatability confirmation for A5 the filtration occurred quite often (Figure 16 a and b). The test repeatability can be assumed to be successful only by measuring points at 40µm, 60.2µm and 120µm apertures. The grout front propagation measurements showed better results (Figure 17).

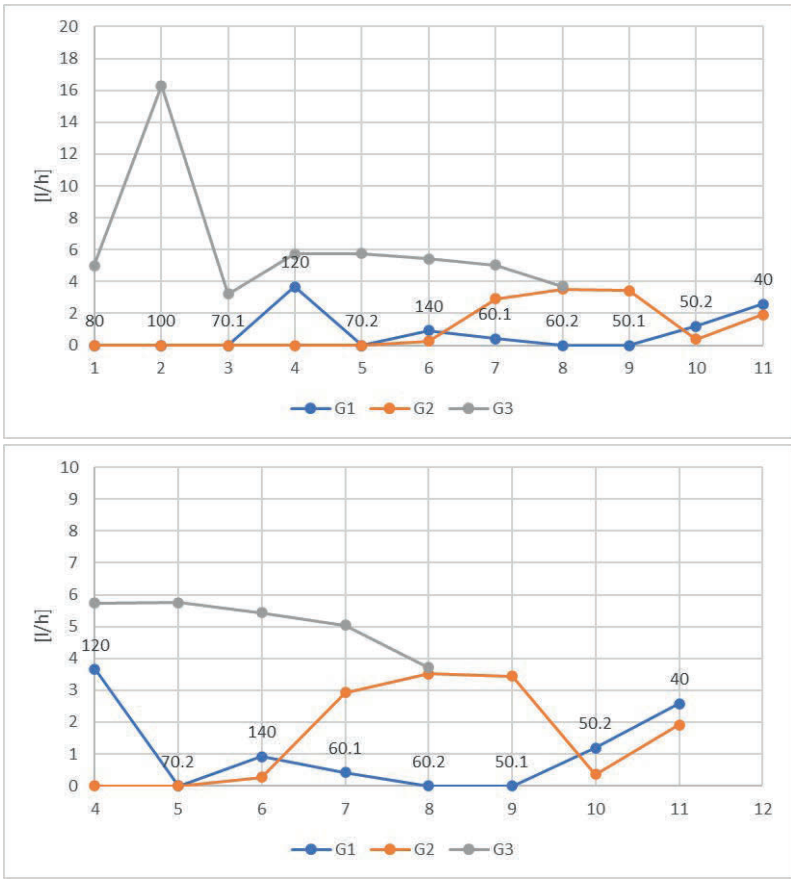

Figure 16. The grout flow rate at each aperture of A5: the graph for all apertures (a) and graph for small apertures at the end of VALS II (b).

Here G3 test was only partially successful and was not used for calculation of average time values of grout propagation over distance.

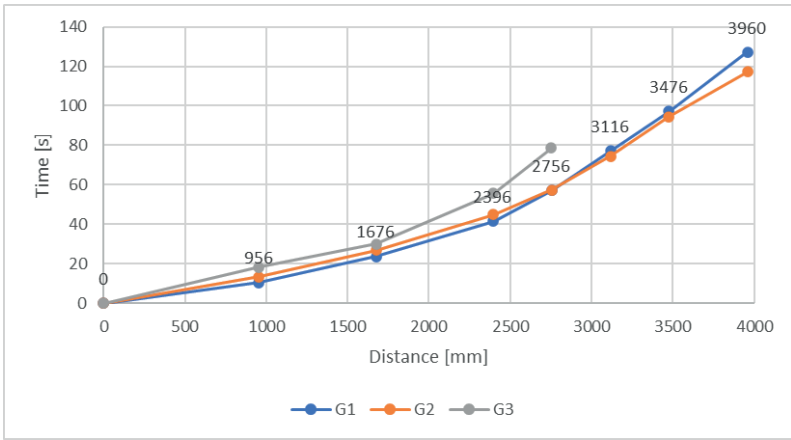

(a)

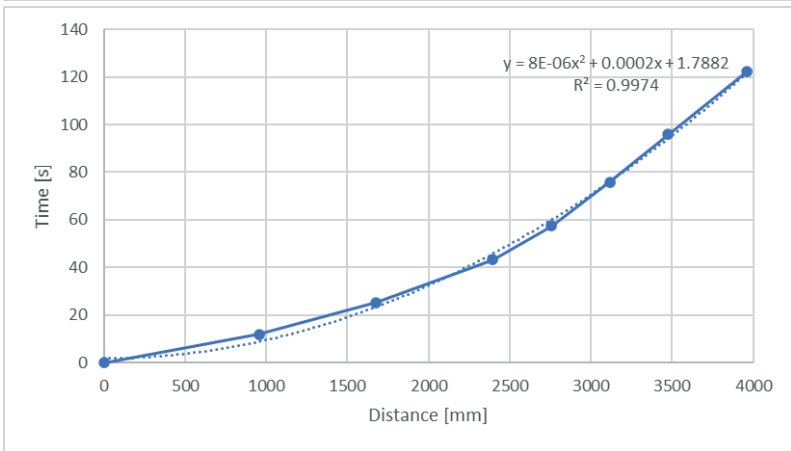

(b)

Figure 17. Recorded grout front propagation in A5: the graph for all tests (a) and average values with fitted function with excluded G3 (b).

3.2.3 Aperture distribution A1

Based on results of A1 water tests, when calculating average value of water flow rate at VALS II outlet W5 results were excluded. The other test repetitions were quite consistent.

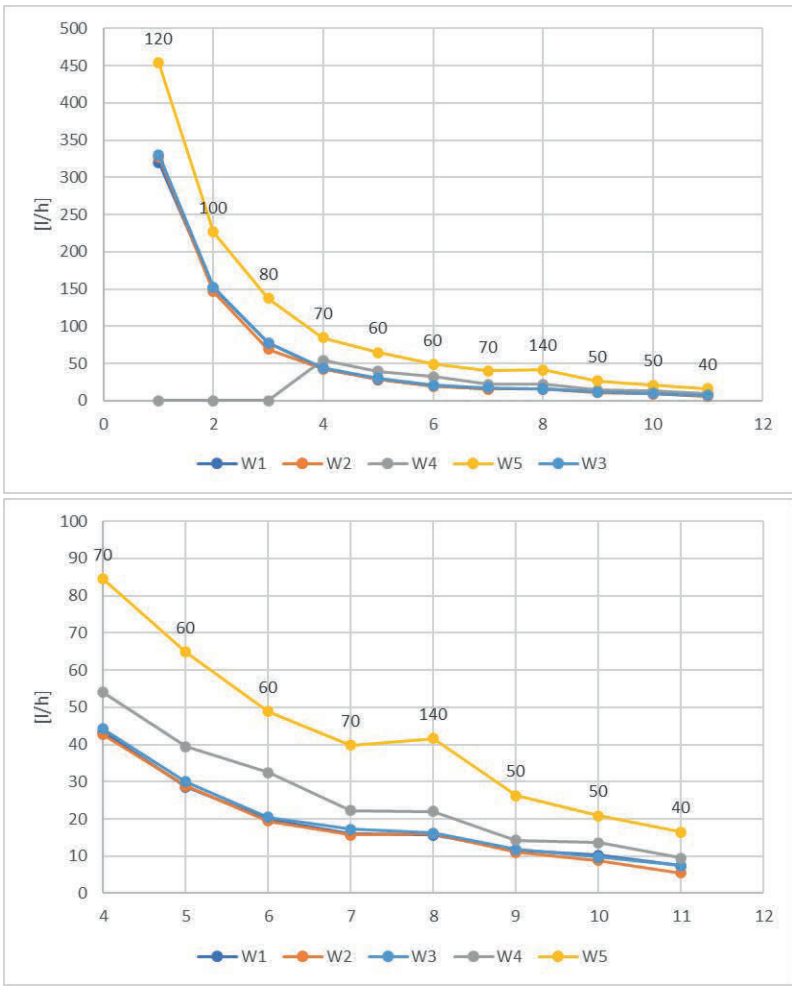

Figure 18. The water flow rate at each aperture of A1: the graph for all apertures (a) and graph for small apertures at the end of VALS II (b).

When measuring grout flow rate during test G4 there was data recording failure for mass sensor signal (Figure 19), however the G4 results were included during grout propagation analysis.

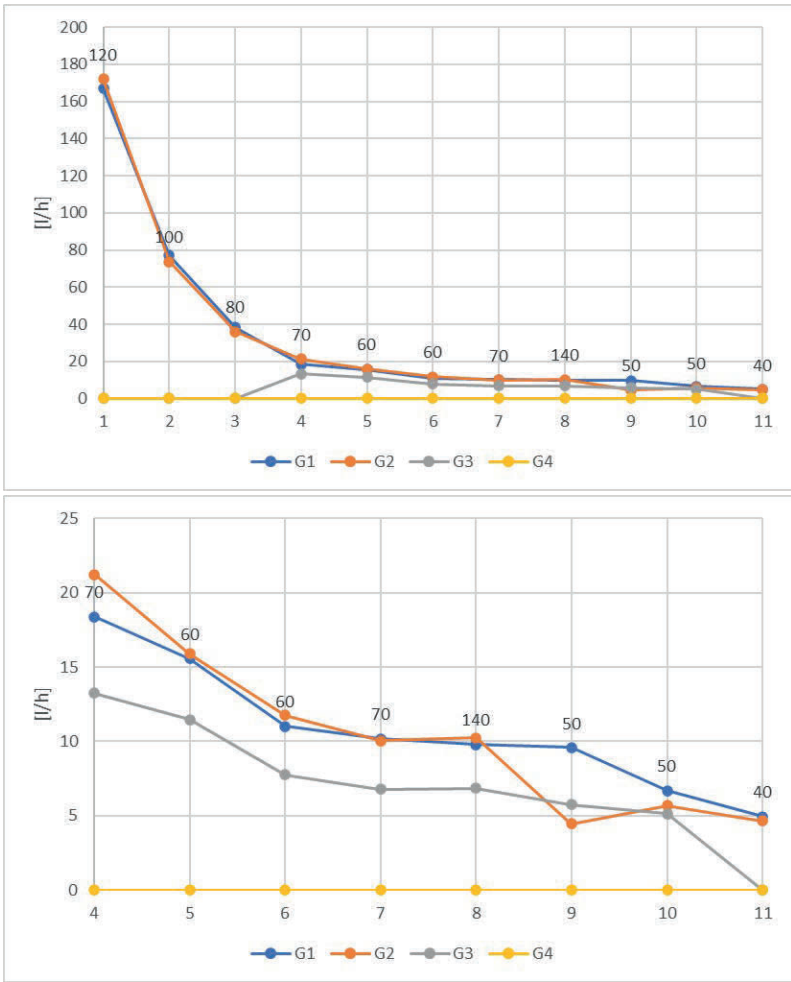

Figure 19. The grout flow rate at each aperture of A1: the graph for all apertures (a) and graph for small apertures at the end of VALS II (b).

Despite of mass sensor failure, the grout front propagation recording for G4 test were successful. The test repeatability was stable at first half of VALS II from inlet.

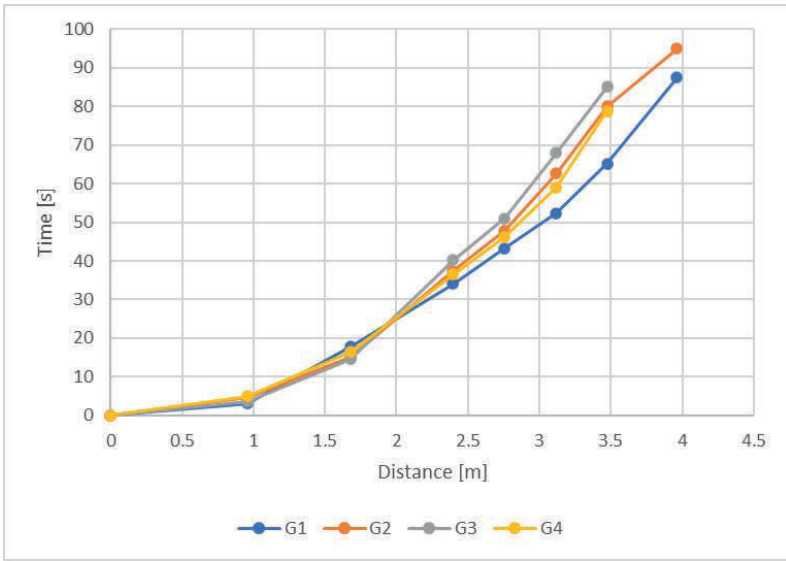

(a)

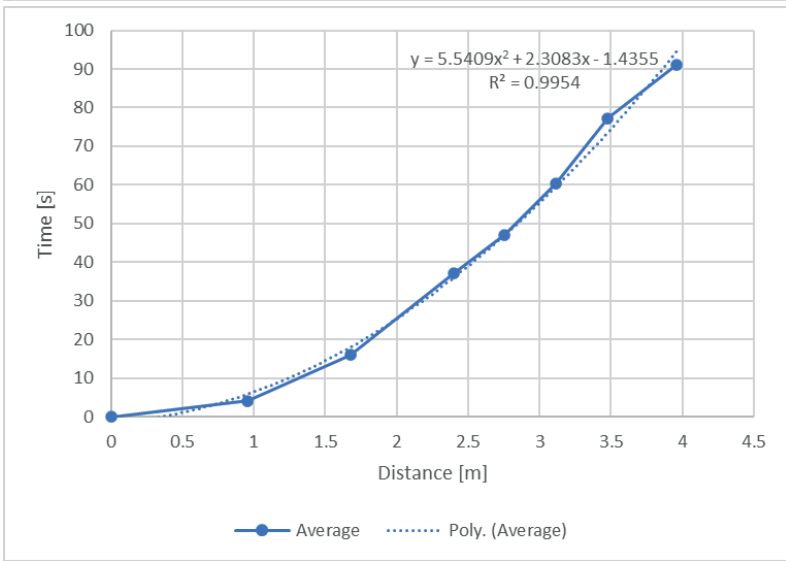

(b)

Figure 20. Recorded grout front propagation in A1: the graph for all tests (a) and average values with fitted function (b).

3.3 Experimental data summary

3.3.1 Grout rheology test

Grout rheology test summary shows that all grout mixes experienced linear increase of plastic viscosity over time (Figure 21). Grout mixes for A2 showed faster increase, which can be explained by lower w/c ratio (see section 4.2). Grout mixes for alternatives A1 and A5 showed similar properties, with somewhat faster increase of plastic viscosity in time frame from 20 min to 30min.

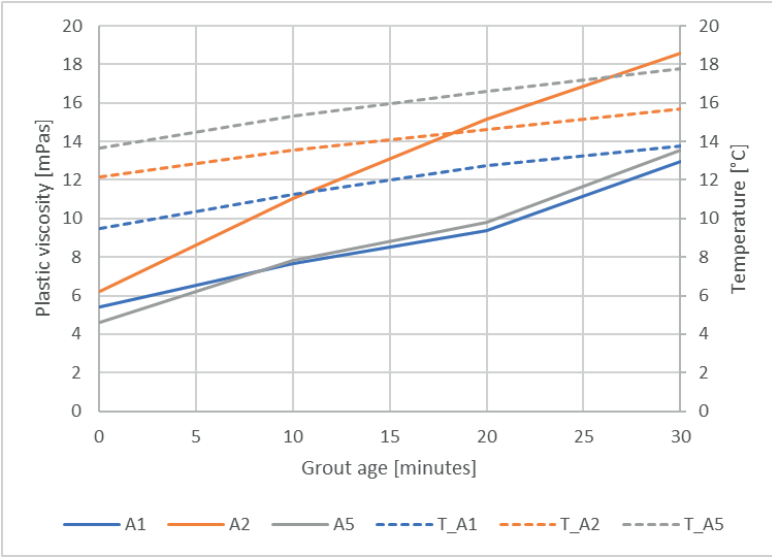

Figure 21. Measured average plastic viscosity and temperature of grout over time for all aperture distribution alternatives.

3.3.2 Grout front propagation

From average data of grout front propagation (Figure 22) grout propagation for A2 showed steeper curve compared to A1 and A5, which can also be explained by lower w/c ratio and thus higher grout plastic viscosity. A1 and A5 exhibit similar behavior with A1 grout propagation being faster. Assumingly this is due to random pattern of aperture distribution in A5 (Figure 10) which should create higher friction loss thus to slow down grout front propagation.

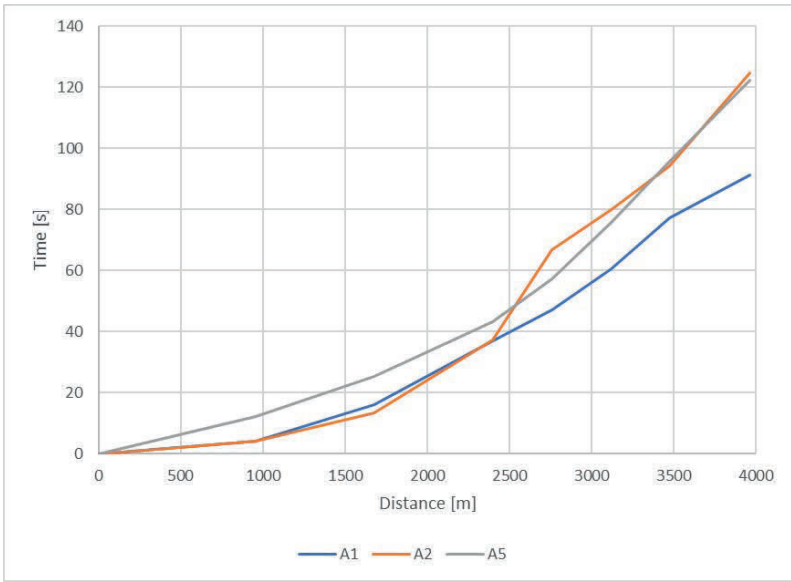

(a)

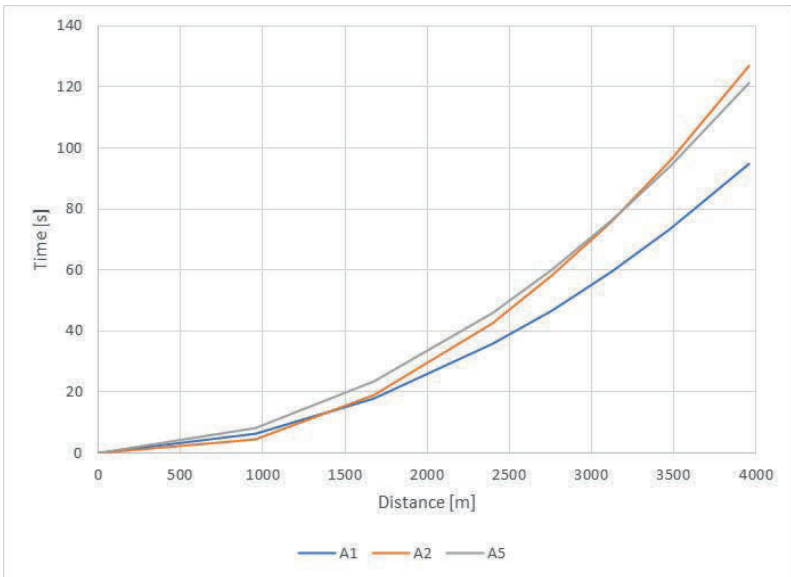

(b)

Figure 22. Average **g**rout front propagation over time in all aperture distribution alternatives: the average data (a) and function (b).

4. ANALYTICAL AND NUMERICAL EVALUATION

4.1 Analytical evaluation

Analytical evaluation of grout propagation prediction based on RTGC theory was done using calculation procedure described in (Ghafar 2017).

After recording water flow rate at the outlet of VALS II during water injection test hydraulic aperture b_h of aperture distribution was deduced from following equation:

$$Q = \frac{\rho_w \cdot g}{12 \cdot \mu_w} \cdot w \cdot b_h^3 \cdot \frac{H}{L} \qquad \textbf{Eq. 1}$$

Where:

Q is the volumetric flow rate, $\frac{m^3}{s}$;

ρ_w the density of water, $\frac{kg}{m^3}$;

μ_w is the dynamic viscosity of water (0.0013 $Pa \cdot s$).

g the acceleration due to gravity, $\frac{m}{s^2}$;

w is the width of aperture, m;

H is the sum of the head losses between the inlet and outlet located at distance L (see Appendix section Figure 28), m.

To determine the grout propagation using RTGC theory the characteristic grouting time t_0 (the time for reaching 80% of the possible penetration length), the relative grouting time t_D and the relative grout penetration length I_D were calculated according Eq. 2, Eq. 3 and Eq. 4:

$$t_0 = \frac{6 \cdot \Delta p \cdot \mu}{\tau_0^2} \qquad \textbf{Eq. 2}$$

$$t_D = \frac{t}{t_0} \qquad \textbf{Eq. 3}$$

$$I_D = \frac{I}{I_{max}} \qquad \textbf{Eq. 4}$$

Where:

Δp is the difference between the grouting pressure and the resisting water pressure, Pa;

μ is the plastic viscosity of grout measured during experiment, $Pa \cdot s$;

τ_0 is the yield stress of grout measured during experiment, Pa;

I the grout penetration length at time t, m;

I_{max} is the maximum penetration length, m;

I_{max} was calculated using Eq. 5

$$I_{max} = \frac{\Delta p \cdot b_h}{2 \cdot \tau_0} \quad \textbf{Eq. 5a}$$

$$I_{max} = \frac{\Delta p \cdot b_{phy}}{2 \cdot \tau_0} \quad \textbf{Eq. 5b}$$

Where:

b_h is hydraulic aperture size, m;

b_{phy} is physical aperture size, m;

To calculate I versus t, the relation between I_D and t_D was approximated for one dimensional (1D) flow condition using Eq. 6 and Eq. 7:

$$\theta_{1D} = \frac{t_D}{2 \cdot (0.6 + t_D)} \quad \textbf{Eq. 6}$$

$$I_D = \sqrt{\theta_{1D}^2 + 4 \cdot \theta_{1D}} - \theta_{1D} \quad \textbf{Eq. 7}$$

The convenient way to summarise the calculation sequence for determining I according RTGC theory is a flow chart by (Ghafar 2017):

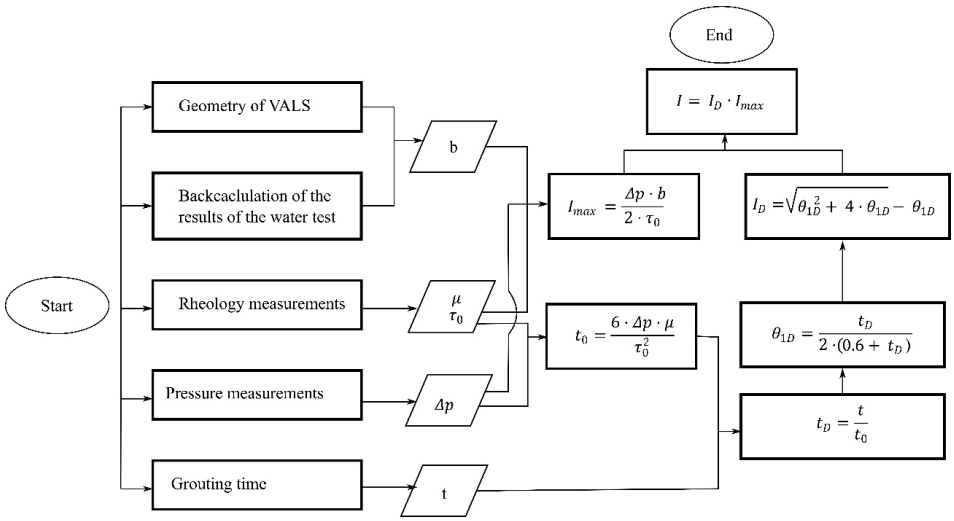

Figure 23. Flow chart used in estimation of grout flow propagation according to RTGC theory **(**Ghafar 2017).

4.2 Numerical evaluation

In the VALS II, the propagation of injected cement grout is an immiscible two-phase flow process, where the injected cement grout displaces air (dry condition) or water (saturated condition) in the long slot. Since the width and aperture of the VALS II are much smaller compared to the length, the propagation process of injected cement grout can be modeled as 1D unidirectional two-phase flow. In our previous work, a two-phase flow model for grout propagation into water-saturated fractures has been developed (Zou et al., 2018; 2020)(Zou, Håkansson and Cvetkovic 2018); (Zou, Håkansson and Cvetkovic 2020), expressed as

$$\frac{\partial}{\partial \mathrm{x}} T(C) \frac{\partial \mathrm{P}}{\partial \mathrm{x}} = 0 \qquad \textbf{Eq. 8}$$

$$u = \frac{T(C)}{2B} \frac{\partial \mathrm{P}}{\partial \mathrm{x}} \qquad \textbf{Eq. 9}$$

$$\frac{\partial C}{\partial t} + u \frac{\partial C}{\partial \mathrm{x}} = 0 \qquad \textbf{Eq. 10}$$

Eq. 8 represents the mass conservation, Eq. 9 determines the propagation velocity of the cement grout, and Eq. 10 represents the phase transport of the two-phase flow process. In these equations, C is a phase function (i.e., C = 1 denotes the grout phase and C = 0 denotes the water or air phase), t is time, P is pressure, u is velocity, and T(C) is the

transmissivity, which is a function of C, depending on the fluid. For groundwater, i.e., C = 0, the transmissivity is given by the cubic law,

$$T(C=0) = -\frac{2WB^3}{3\mu_w} \qquad \textbf{Eq. 11}$$

where B is the half of the fracture aperture, i.e., B=b/2, W is the fracture width and μ_w is the viscosity of groundwater. Since this numerical model considers the variable apertures, the aperture b represents the physical (mechanical) aperture.

The rheological properties of cement grouts are greatly dependent on water and cement ratios. In practice, the water and cement ratio are between 0.6 and 0.8, where the cement grouts behave as yield-stress fluids, often approximated by the Bingham model, expressed as

$$\begin{cases} \tau = \tau_0 + \mu_g \dot{\gamma}, & |\tau| > \tau_0 \\ \dot{\gamma} = 0 & \text{otherwise} \end{cases} \qquad \textbf{Eq. 12}$$

where τ is shear stress, τ_0 is the yield stress, μg is the plastic viscosity and $\dot{\gamma}$ is the shear rate.

For the Bingham grout, its transmissivity can be determined by the analytical solution of the flowrate for single-phase flow between smooth parallel plates, expressed as (Zou et al., 2018) (Zou, Håkansson and Cvetkovic 2018)

$$T(C=1) = -\frac{WB^3}{3\mu_g}\left(1-\frac{z_p{}'}{B}\right)^2\left(2+\frac{z_p{}'}{B}\right) \qquad \textbf{Eq. 13}$$

where zp' is half of the plug flow region in the grout phase, which is a function of yield stress and the pressure gradient between the injection inlet and grout propagation front I(t) (Zou et al., 2018) (Zou, Håkansson and Cvetkovic 2018)

$$z_p{}' = min\left(\frac{\tau_0 \mathrm{I(t)}}{P_1 - P_{\mathrm{I(t)}}}, B\right) \qquad \textbf{Eq. 14}$$

where PI(t) is the pressure at the interface. Illustration of the plug flow region for yield stress fluid flow in homogeneous fractures is available in (Zou, Håkansson and Cvetkovic 2018).

The mathematical model for the two-phase flow of cement grout propagation in the VALS is a set of nonlinear partial differential equations, since the transmissivity for the Bingham grouts is naturally nonlinear. For modeling of grout propagation in fractures with variable aperture structures, the mathematical model is solved numerically by iteration at each time step. To track the propagation interface, a novel algorithm by introducing a moving node in each fracture has been developed in (Zou et al., 2018) (Zou, Håkansson and Cvetkovic 2018). The detailed algorithm of the solution for the two-phase flow of grout

propagation in saturated fracture networks and its advantages compared to traditional methods can be found in (Zou et al., 2018) (Zou, Håkansson and Cvetkovic 2018).

Specifically, a Galerkin finite element method (FEM) code using the Picard iterative method is developed to solve for the two-phase flow of cement grout propagation in the VALS. The FEM - rather than iteratively solving the pressure at the interface by using the flowrate equation - is used because of its advantages in consideration of complex geometry of the VALS with spatially varying apertures. At each time step, the mesh is refined by adding one node at the interface, so that only one pressure value is directly solved at the interface node without need for subsequent interpolation; this ensures continuity of the pressure field at the interface. The velocity is then calculated by Eq. 9 after obtaining a convergent pressure field.

The phase transport is a hyperbolic (advection) equation, which is a difficult numerical problem in the presence of a sharp interface (i.e. high phase gradient) at the grout front if a Eulerian scheme is used. To overcome this numerical difficulty, a Lagrangian interface tracking method was adopted to track the grout penetration. The advective interface transport follows the motion equation and is written as

$$I^{n+1} = I^n + u(I^n)\Delta t \qquad \textbf{Eq. 15}$$

where I is the position of the interface and Δt is the time step. Since Eq. 8, Eq. 9 is an explicit discretization scheme, the adaptive time step based on the Courant-Friedrichs-Levy (CFL) condition is used in this study to achieve higher efficiency and maintain computational stability for the solution, expressed by

$$\Delta t \leq \frac{\Delta x}{u} \qquad \textbf{Eq. 16}$$

where Δx is a characteristic length assumed to be the mesh size.

This two-phase flow model and the associated solution method have been validated against analytical solution for the special case of a two Newtonian fluids flow problem, presented in (Zou et al., 2018) (Zou, Håkansson and Cvetkovic 2018). In this project, we use this two-phase flow model to conduct numerical evaluation of the grouting tests in the VALS.

5. LABORATORY MEAUSREMETS VS. RTGC THEORY AND NUMERICAL PREDICTION

5.1 Aperture distribution A2

The calculation of RTGC theory prediction for grout propagation based on experimentally obtained data first was done using grout rheology measurements at 0 minutes after grout mixing (Figure 24a). Two calculations for grout propagation prediction were done, one using physical average aperture size of A2 distribution b_{phy} and other one using hydraulic aperture b_h obtained from water tests.

As it is seen from graph RTGC results using b_{phy} highly overestimates grout propagation speed. When using b_h RTGC prediction is closer to test results but still the overestimation for grout propagation is rather high.

Numerical simulation results however also overestimate grout propagation speed and are more like RTGC b_h prediction. It should be noted that for numerical simulations at grout age of 0 minutes grout properties of 5 minutes were used instead, since that was usual grout age when data recording in laboratory test started.

To improve RTGC prediction on grout propagation grout rheological data used from later measurements after mixing. It was found that when using grout rheology at 30 minutes age RTGC b_h prediction is rather close to experimental results (Figure 24 b). with some underestimation for grout propagation. This suggests that grout rheology properties at time between 20 and 30 minutes should be used for more accurate RTGC prediction. Moreover, the numerical simulation results are also improved, while RTGC b_{phy} here is still far from experimental results.

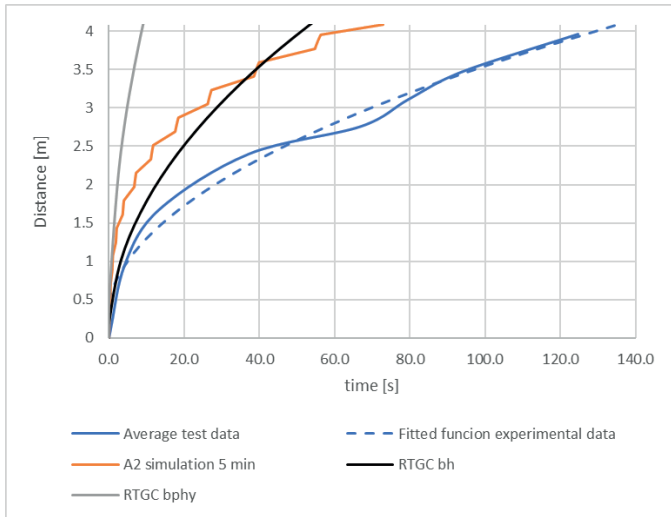

(a)

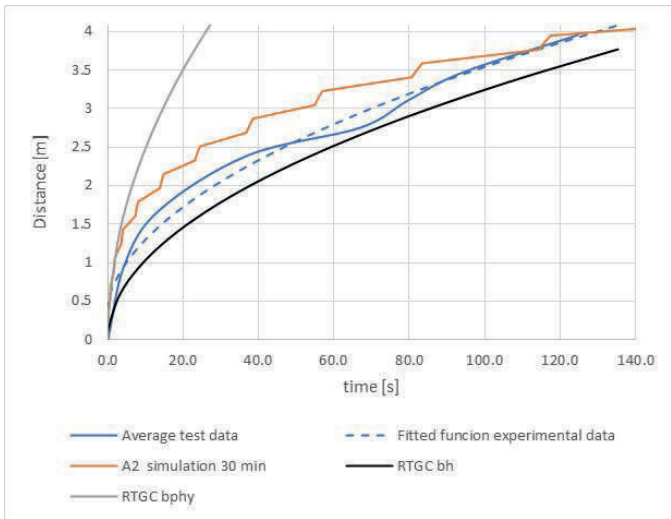

(b)

Figure 24. RTGC analysis and numerical simulation results for alternative A2 using grout rheology measurements as 0 minute after mixing (a) and 30 minutes after mixing (b).

5.2 Aperture distribution A5

The results of RTGC analysis on alternative A5 confirms findings for aperture distribution A2 tests. Here RTGC b_h prediction and numerical analysis with rheology of 0 minutes overestimates grout propagation compared to laboratory results (Figure 25a), while calculations based on 30 minutes grout rheology gives very good match for RTGC b_h with experimental results (Figure 25b) and slight overestimation for numerical simulation. For b_{phy} again in both cases RTGC gives overestimated propagation predictions.

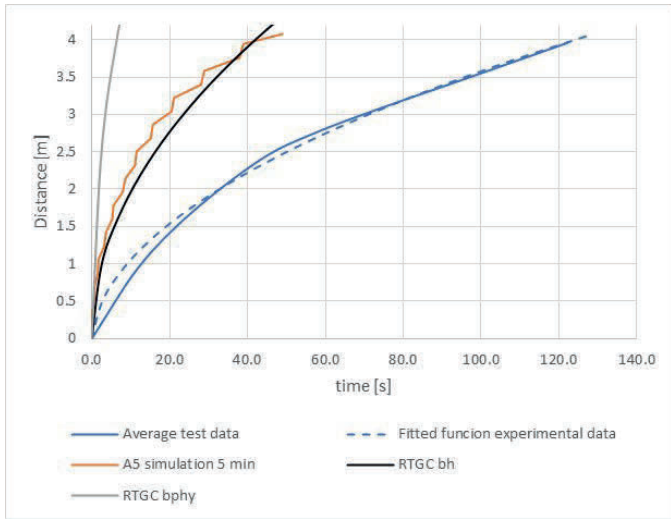

(a)

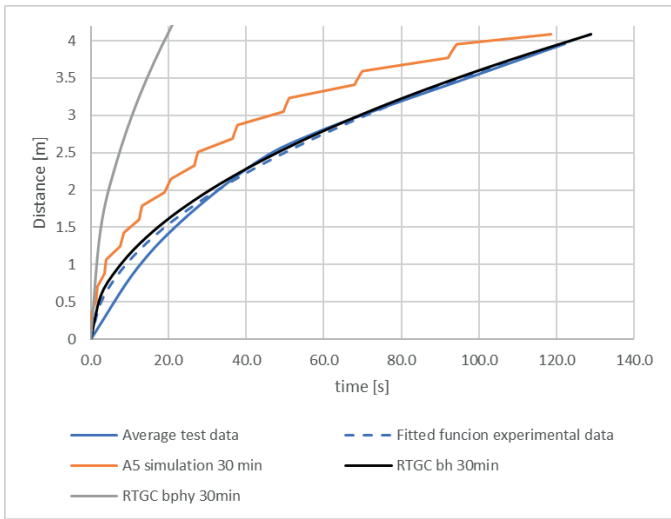

(b)

Figure 25. RTGC analysis and numerical simulation results for alternative A5 using grout rheology measurements as 0 minute after mixing (a) and 30 minutes after mixing (b).

5.3 Aperture distribution A1

RTGC b_h prediction and numerical analysis for A1 closely follows findings for A5, although some under-estimation can be observed for RTGC b_h at propagation time of 100 seconds (Figure 26b). This suggests that extrapolated grout properties between 20 and 30 minutes should be used.

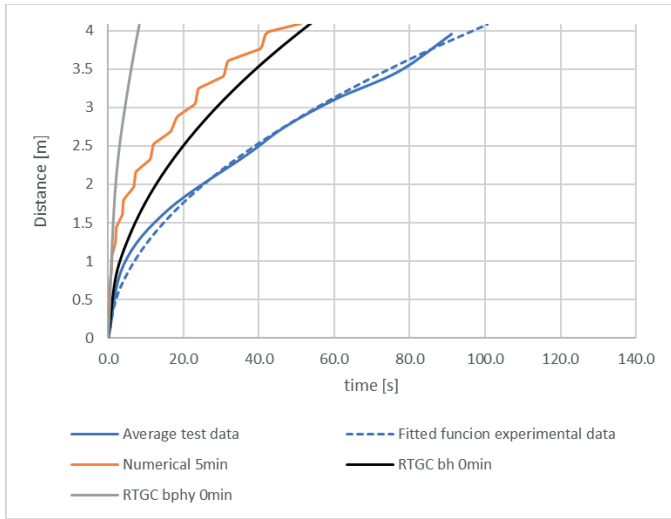

(a)

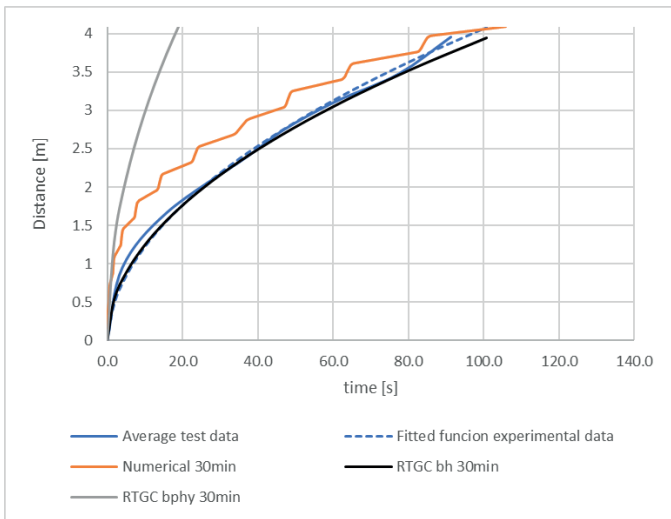

(b)

Figure 26. RTGC analysis and numerical simulation results for alternative A1 using grout rheology measurements as 0 minute after mixing (a) and 30 minutes after mixing (b).

6. DISCUSSIONS

In this project, the improved Variable Aperture Long Slot (VALS) version II was successfully designed and manufactured to test cement grout propagation, which is used to validate the RTGC method applied for variable aperture size distributions in a 1D fracture. Three representative scenarios of variable aperture distributions (A1, A2, and A5) of grouting tests were conducted using the VALS II. Those tests provide valuable data for validating predictive models for rock grouting analysis. In particular, the analytical results predicted by RTGC method using both physical aperture and hydraulic aperture were calculated for comparison with the experiments. Numerical simulations based on a two-phase flow model were also conducted for comparison. The results generally indicate that the RTGC method can roughly predict the propagation distance after calibration of the rheological properties using the parameters measured at 10 or 30 minutes after mixing. The proposed research objectives are fulfilled.

Moreover, during the experimental testing with grout using VALS II the filtration phenomena was observed. It should be noted that the investigation of filtration was not within the scope of the research and more tests would be needed for a thorough investigation. However, initial observations suggest that most often filtration occurred for when performing experiments on aperture distribution A2 using lower w/c ratio grout mix (w/c=0.9). When comparing a filtration occurrence for a grout mix with same w/c ratio for the aperture distributions A1 and A5, a filtration occurred for A5 more often, i.e. for aperture distribution with larger constrictions.

It is worth mentioning that the cement propagation processes are complex due to the combined effects of rock fracture geometry and cement grout rheological properties. There are complex fracture networks in rock masses with multiple scales of heterogeneity, i.e., structural scale heterogeneity, fracture-to-fracture scale heterogeneity, and single fracture scale heterogeneity. Those multiple scales of heterogeneity significantly affect fluid flow in fractured rock (Zou and Cvetkovic 2020). It is expected that those multiple scales of heterogeneity will also affect the cement grout propagation process. In this study, we considered different aperture size distributions in the long slot, which can represent cement grout propagation into connected fractures with different aperture sizes. It demonstrates the impact of fracture-to-fracture scale heterogeneity. The impacts of structural scale and single fracture scale heterogeneities on cement grout propagation remain important topics for future studies.

Meanwhile, the measurements of cement grout rheological properties show considerable variations and time-dependent behaviours. Using more accurate rheological models, such as Herschel–Bulkley model (Zou, Tang and Li 2024) and applying more accurate measurement methods, such as in-line rheological measurements using Ultrasound Velocity Profiling combined with the Pressure Difference (UVP + PD) method (Rahman, Håkansson and Wiklund 2015) could be more suitable in cement grouting research and engineering practice.

7. CONCLUSIONS

The improved version of VALS II was successfully designed and constructed. VALS II is proved to be tight for both, water and grout testing under pressure. The results had good repeatability showing that after each new assembly of VALS II, the designed aperture size remains similar.

The laboratory grouting tests using VALS II revealed that filtration phenomenon was rather frequent. Most frequently it happened for cement grout with lower w/c ratio for aperture distribution A2 and when comparing test with grout of same w/c ratio it happened more frequently for aperture distribution A5, i.e. having larger of geometry constrictions compared to A1.

When measuring grout propagation at aperture distributions it was observed to be slower for alternative with higher constrictions A5 compared to A1, while the slowest grout propagation was observed for lower w/c ratio grout at aperture distribution A2.

Although the grout propagation in rock fractures is governed by physical aperture b_{phy} the comparison of RTGC predictions to experimental results proved that hydraulic aperture b_h should be used for calculations of the front propagation distance.

RTGC b_h prediction overestimates grout propagation over time compared with laboratory results if grout rheological properties at 0 minutes are used. When grout rheological properties at 30 minutes after mixing is used the RTGC b_h predictions match tests results very well.

Numerical simulation of grout propagation results based on the physical variable apertures gives more accurate prediction results compared to the RTGC solution based on physical aperture. However, the numerical results still overestimated penetration distance compared to experimental test results. The main reason for the slight overestimation compared to the experimental results is that the time-dependent (continuously changing) rheology properties and the additional friction loss caused by inertial effects are not considered in the numerical simulations. Those effects could be lumped into the RTGC predictions by using the hydraulic aperture.

ACKNOWLEDGEMENT

This project received funding from Bergteknisk Forsking Foundation (BeFo), the Swedish Building Industry Development Fund (SBUF) and RISE. We would like to acknowledge Master Builders Solutions Sverige AB with help on materials and mix design development and Heidelberg Materials Cement Sverige AB for providing materials. Working group members Maria Golubeva, Norrstrand, Muje Kiqina, Thed Hendriksson and Markus Abrahamsson helped in the laboratory and Ulf Håkansson, Ali Nejad Ghafar and Almir Draganović for helping discussion during design of VALS II. Ida Gabrielsson for helping with translation.

8. REFERENCES

Axelsson, Magnus, Gunnar Gustafson, and Åsa Fransson. 2009. “Stop mechanism for cementitious grouts at different water-to-cement ratios.” *Tunnelling and Underground Space Technology* 24 (4): 390-397.

Draganović, Almir, and Håkan Stille. 2011. “Filtration and penetrability of cement-based grout: Study performed with a short slot.” *Tunnelling and Underground Space Technology* 26 (4): 548-559. doi:https://doi.org/10.1016/j.tust.2011.02.007.

Ghafar, A. N. 2017. *An Experimental Study to Measure Grout Penetrability, Improve the Grout Spread, and Evaluate the Real Time Grouting Control Theory.* PhD Thesis, Stockholm: KTH Royal Institute of Technology.

Ghafar, Ali, Nejad, Sasan Sadrizadeh, Konstantinos Magakis, Almir Draganović, and Stefan Larsson. 2017. “Varying Aperture Long Slot (VALS), a Method for Studying Grout Penetrability into Fractured Hard Rock.” *Geotechnical Testing Journal* 40. doi:10.1520/GTJ20160179.

Gustafson, Gunnar, and Håkan Stille. 1996. “Prediction of groutability from grout properties and hydrogeological data.” *Tunnelling and Underground Space Technology* 11 (3): 325-332. doi:10.1016/0886-7798(96)00027-2.

Gustafson, Gunnar, and Håkan Stille. 2005. “Stop Criteria for Cement Grouting.” *Felsbau: Zeitschrift Für Geomechanik Und Ingenieurgeologie Im Bauwesen Und Bergbau* 23 (3): 62-68.

Gustafson, Gunnar, Johan Claesson, and Åsa Fransson. 2013. “Steering Parameters for Rock Grouting.” *Journal of Applied Mathematics* 1-9. https://doi.org/10.1155/2013/269594.

Håkansson, U. 1993. *Rheology of Fresh Cement-Based Grouts.* PhD Thesis, Stockholm: Royal Institute of Technology.

Kobayashi, Shinji, Håkan Stille, and Gunnar Gustafson. 2008. *Real Time Grouting Control Method: Development and application using Äspö HRL data.* SKB Rapport, Stockholm: Royal Institute of Technology KTH.

Rahman, M., U Håkansson, and J. Wiklund. 2015. “In-line rheological measurements of cement grouts: Effect of water/cement ratio and hydration.” *Tunnelling and Underground Space Technology* 45: 34-42. doi:https://doi.org/10.1016/j.tust.2014.09.003.

Saeidi, Omid, Håkan Stille, and Seyed Rahman Torabi. 2013. “Numerical and analytical analyses of the effects of different joint and grout properties on the rock mass

groutability." *Tunnelling and Underground Space Technology* 38: 11-25. https://doi.org/10.1016/j.tust.2013.05.005.

Stille, H., G. Gustafson, and L. Hassler. 2012. "Application of New Theories and Technology for Grouting of Dams and Foundations on Rock." *Geotechnical and Geological Engineering* 603-624. https://doi.org/10.1007/s10706-012-9512-7.

Stille, Håkan. 2015. *Rock Grouting - Theories and Applications.* Rock Engineering Research Foundation BeFo.

Tsuji, M., M. Holmberg, B. Stille, J.Y. Rafi, and H. Stille. 2012. *Optimization of the grouting procedure with RTGC method. Data from a trial grouting at city line project in Stockholm.* Stockholm: Svensk Kärnbränslehantering AB (SKB).

Zimmerman, R., and Gudmundur Bodvarsson. 1996. "Hydraulic conductivity of rock fractures." *Transport in Porous Media* 23: 1-30. doi:10.1007/BF00145263.

Zou, L., and V. Cvetkovic. 2020. "Inference of transmissivity in crystalline rock using flow logs under steady-state pumping: Impact of multiscale heterogeneity." *Water Resources Research* 56 (8). doi:https://doi.org/10.1029/2020wr027254.

Zou, L., M. Tang, and B. Li. 2024. "Bingham and Herschel-Bulkley fluids flow regimes in rough-walled rock fractures." *International Journal of Rock Mechanics and Mining Sciences.* doi:https://doi.org/10.1016/j.ijrmms.2024.105832.

Zou, Liangchao, Ulf Håkansson, and Vladimir Cvetkovic. 2020. "Analysis of Bingham fluid radial flow in smooth fractures." *Journal of Rock Mechanics and Geotechnical Engineering* 12 (5): 1112-1118. doi:https://doi.org/10.1016/j.jrmge.2019.12.021.

Zou, Liangchao, Ulf Håkansson, and Vladimir Cvetkovic. 2018. "Two-phase cement grout propagation in homogeneous water-saturated rock fractures." *International Journal of Rock Mechanics and Mining Sciences* (International Journal of Rock Mechanics and Mining Sciences) 106: 243-249. doi:https://doi.org/10.1016/j.ijrmms.2018.04.017.

9. APPENDIX

9.1 Drawings of VALS II components

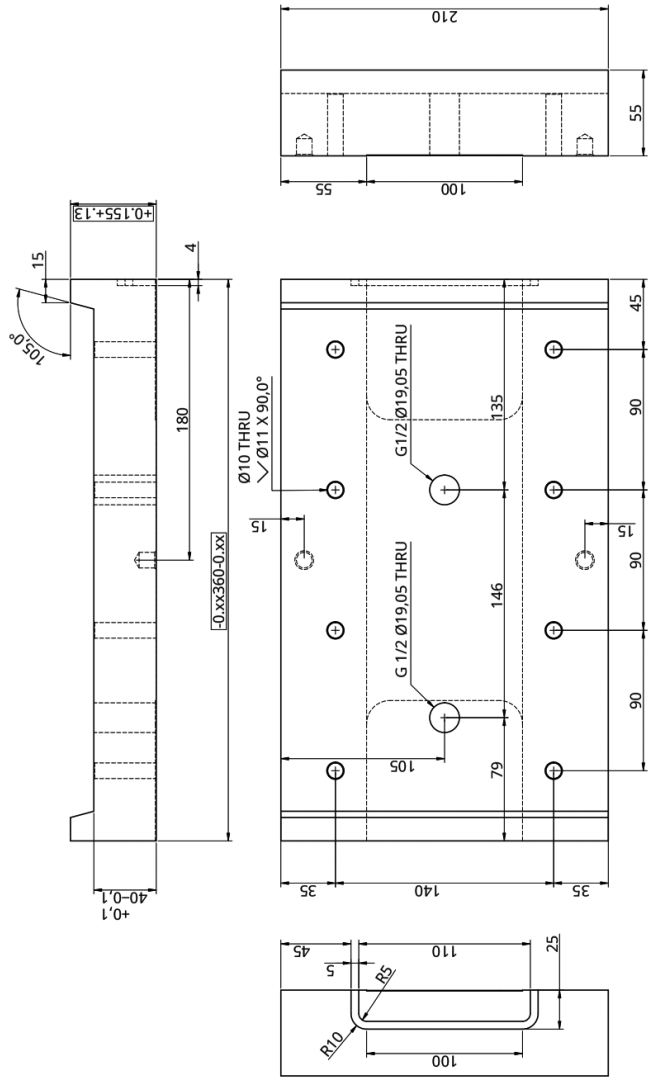

Figure 27. Drawing of aperture plate.

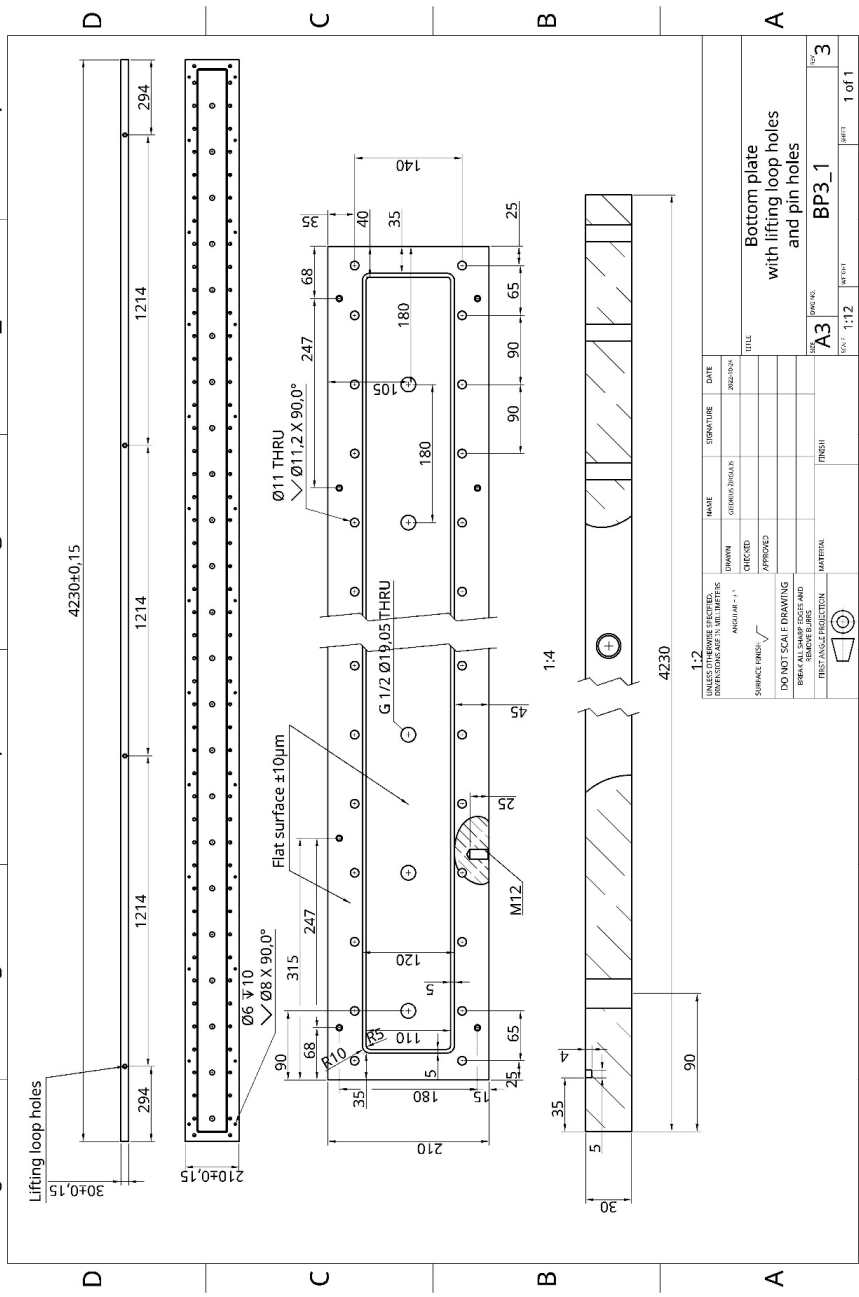

Figure 28. Drawing of bottom plate.

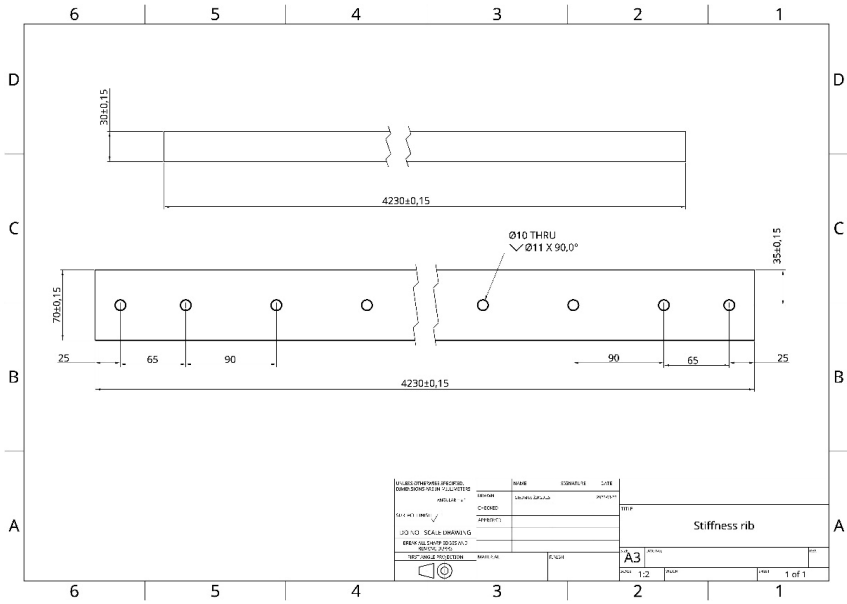

Figure 29. Drawing of the stiffness rib.

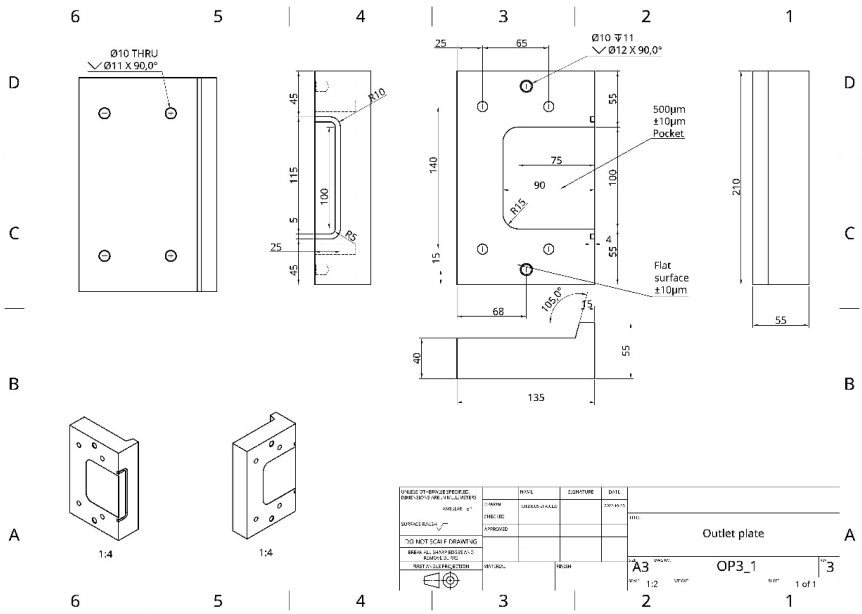

Figure 30. Drawing of the outlet plate.

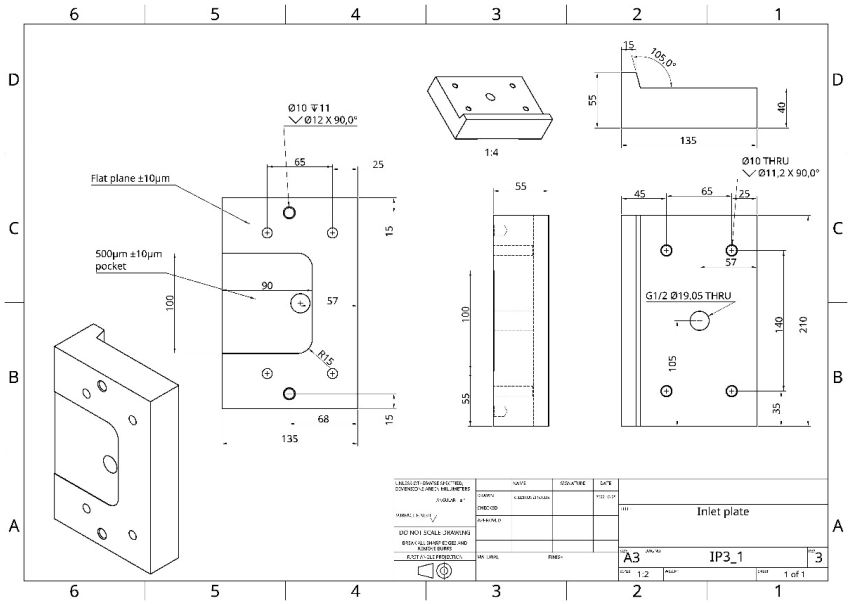

Figure 31. Drawing of the inlet plate.

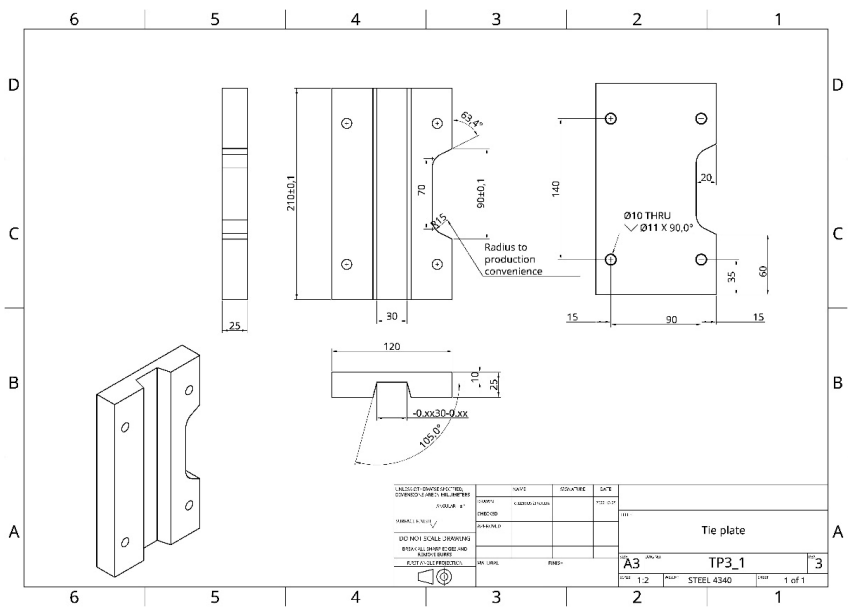

Figure 32. Drawing of the tie plate.

9.2 Images of test setup

Figure 33. Mass sensor with bucket for grout flow recording.

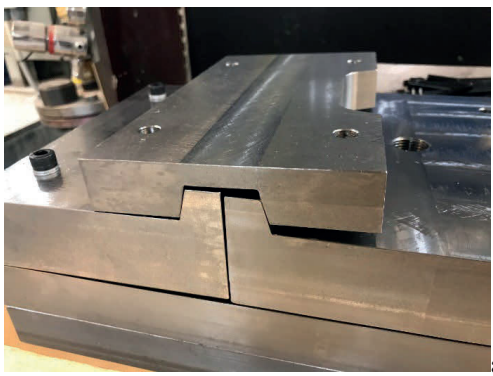

a

b

Figure 34. Gradual tightening of tie plate: before tightening (a) and fully tightened tie plate and adjacent aperture plate (b).

Figure 35. The junction of O-ring for sealing side of aperture plate and O-ring for sealing bottom plate. The good seal between both O-rings after tightening plates is important for successful water test.

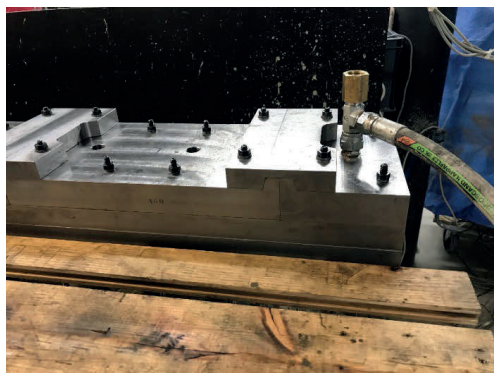

Figure 36. Upgraded position of the grout inlet hose. The top entrance of "T" connection is used for installation pressure sensor.

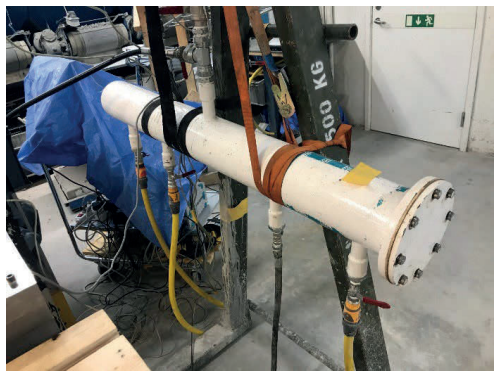

Figure 37. Distribution unit which is filled with grout before testing and pressurized with nitrogen.

9.3 Examples of failed hydraulic test

Figure 38. Example of water leakage during experiments for finding correct O-ring hardness. Water stream between aperture plates (a) and multiple water streams along connection between aperture plates and the bottom plate and a strong water jet marked in red (b).

Figure 39. Water failed to reach outlet plate due to plug at the inlet plate. The plug was formed of hardened grout particles carried by water from not clean enough distribution unit walls.

9.4 Location of grout flow valves, pressure sensors and grout inlet

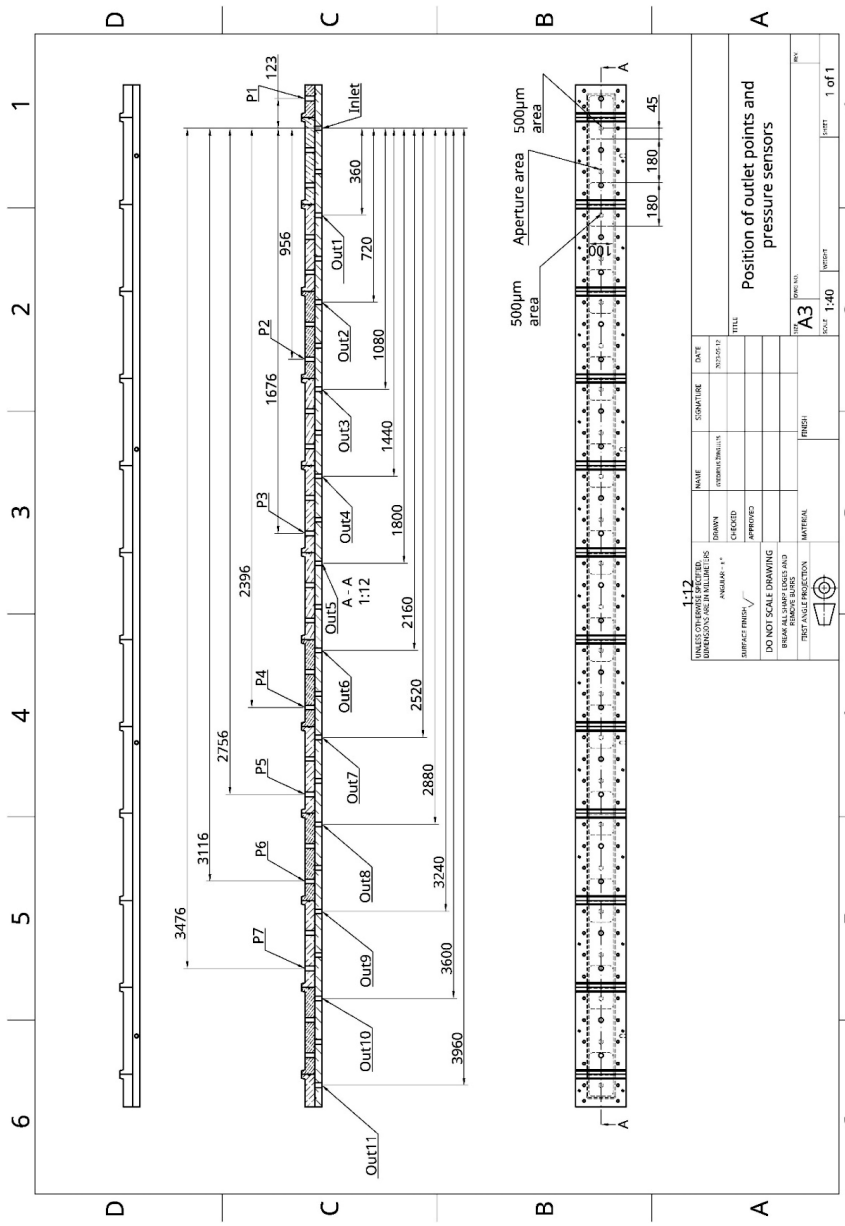

Figure 40. Distance of grout outflow valves and pressure sensors with respect to grout inlet.

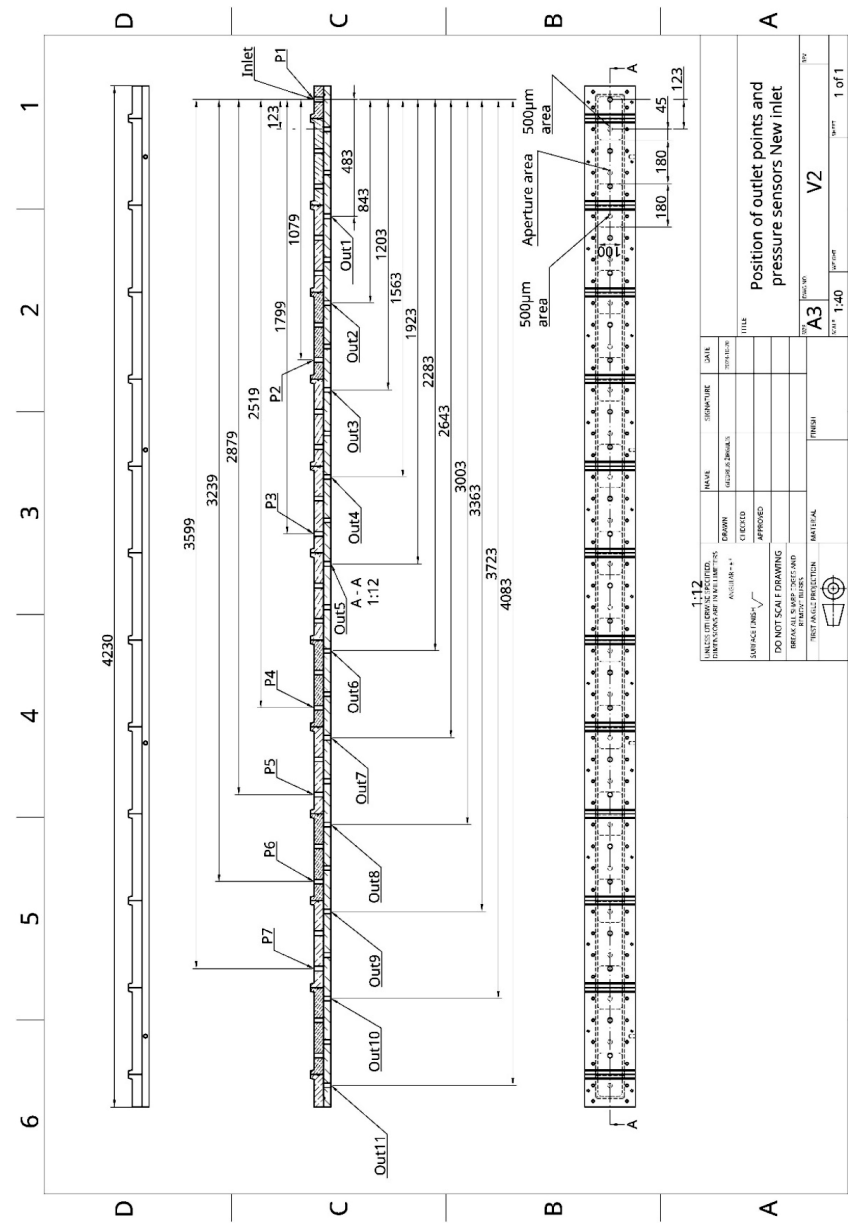

Figure 41. Distance of grout outflow valves and pressure sensors with respect to upgraded grout inlet.

9.5 Calculation example of A2

Input data for hydraulic aperture calculation:

$b_{phy} = 288.2\mu m$

Pressure at inlet: 10 $bars$

Water density $\rho = 1000 \frac{kg}{m^3}$

Dynamic viscosity of water $\mu = 0.0013 Pa \cdot s$

Aperture width, $w = 0.1m$

Calculation of b_h:

$$b_h = \sqrt[3]{\frac{Q}{\frac{\rho g}{12\mu} \cdot w \cdot \frac{H}{L}}}$$

Hydraulic aperture calculations:

outlet number		1	2	3	4	5	6	7	8	9	10	11
distance L, mm		483	843	1203	1563	1923	2283	2643	3003	3363	3723	4083
Aperture, µm		140	120	100	80	70	70	60	60	50	50	40
re b_{phy}, µm		320.0	315.0	310.0	305.0	301.0	298.3	309.3	293.8	291.7	290.0	288.2
Measured Q, l/h		392.1	232.8	140.4	79.4	46.7	31.5	24.0	18.0	14.3	12.0	9.5
	Q, m3/s	0.0	0.0	0.0	0.0	0.0	0.0	0.0	0.0	0.0	0.0	0.0
	ρg/12µ	628846.2	628846.2	628846.2	628846.2	628846.2	628846.2	628846.2	628846.2	628846.2	628846.2	628846.2
	H/L	207.0	118.6	83.1	64.0	52.0	43.8	37.8	33.3	29.7	26.9	24.5
aperture	bh, m	0.0	0.0	0.0	0.0	0.0	0.0	0.0	0.0	0.0	0.0	0.0
	bh, µm	203.0	205.4	195.4	176.4	158.3	147.0	140.9	133.6	128.4	125.5	119.6

After hydraulic aperture is calculated the average physical aperture is calculated simply as arithmetical mean of all apertures and 500µm chambers.

Then the RTGC analysis follows.

Input data for RTGC evaluation:

Inputs	Grout parameters		
	µ	τ	ΔP
	Pa*s	Pa	Pa
0min	0.0062	0.727	1000000
10min	0.0110	0.6445	
30min	0.0186	0.496	

First t_0 is calculated for grout properties at different time:

$$t_0 = \frac{6 \cdot \Delta p \cdot \mu}{\tau_0^2}$$

Time, min	t_0
0	70384.0
10	159372.0
30	453629.0

Then t_D, θ_{1D}, I_D, I_{max} and finally I. t needed for t_D calculation is obtained from fitted function to experimental data, then recalculated for each distance L.

$$t_D = \frac{t}{t_0}$$

$$\theta_{1D} = \frac{t_D}{2 \cdot (0.6 + t_D)}$$

$$I_D = \sqrt{\theta_{1D}^2 + 4 \cdot \theta_{1D}} - \theta_{1D}$$

$$I_{max} = \frac{\Delta p \cdot b}{2 \cdot \tau_0}$$

$$I = I_D \cdot I_{max}$$

RTGC calculations:

								When grout rehology at 0 min of measurements						
		outlet number	inlet	1	2	3	4	5	6	7	8	9	10	11
		distance L, mm	0.00	483.00	843.00	1203.00	1563.00	1923.00	2283.00	2643.00	3003.00	3363.00	3723.00	4083.00
		distance L, m	0.00	0.48	0.84	1.20	1.56	1.92	2.28	2.64	3.00	3.36	3.72	4.08
		Hydraulic aperture bh, m		0.0002030	0.0002054	0.0001954	0.0001764	0.0001583	0.0001470	0.0001409	0.0001336	0.0001284	0.0001255	0.0001196
		Physical aperture bphy, m		0.0003200	0.0003150	0.0003100	0.0003050	0.0003010	0.0002983	0.0002957	0.0002938	0.0002917	0.0002900	0.0002882
	Time from Solver equation [s]		0.00	0.20	3.11	8.38	16.00	25.98	38.32	53.02	70.07	89.49	111.26	135.38
	Relative grouting time	tD	0.000000	0.000003	0.000044	0.000119	0.000227	0.000369	0.000544	0.000753	0.000996	0.001271	0.001581	0.001924
		θ_1D	0.000000	0.000002	0.000037	0.000099	0.000189	0.000307	0.000453	0.000627	0.000828	0.001057	0.001314	0.001598
	Relative penetration length	*I_D*	0.000000	0.003075	0.012098	0.019816	0.027334	0.034762	0.042132	0.049455	0.056738	0.063982	0.071191	0.078363
		Imax, m (bh) (rheolo		139.62	141.29	134.39	121.29	108.86	101.09	96.90	91.87	88.33	86.29	82.22
		Imax, m (bphy)		220.08	216.64	213.20	209.77	207.02	205.18	203.38	202.03	200.60	199.45	198.20
		Imax, m (bh)		*82.2*		*Imax, m (bhy)*	*198.2*							
		I [m] bh	0.0	0.3	1.0	1.6	2.2	2.9	3.5	4.1	4.7	5.3	5.9	6.4
		I [m] bphy	0.0	0.6	2.4	3.9	5.4	6.9	8.4	9.8	11.2	12.7	14.1	15.5

BeFo

Box 5501
SE-114 85 Stockholm

info@befoonline.org • www.befoonline.org
Visiting address: Storgatan 19, Stockholm

ISSN 1104-1773